# Freak waves: Their occurrence and probability

D. Chalikov[a)]
*P. P. Shirshov Institute of Oceanology, Russian Academy of Sciences, Saint-Petersburg Branch, Saint-Petersburg 199053, Russia*

(Received 27 December 2008; accepted 1 June 2009; published online 14 July 2009)

This paper describes the results of more than 4000 long-term (up to thousands of peak wave periods) numerical simulations of nonlinear gravity surface waves performed for the investigation of properties and estimation of statistics of extreme ("freak") waves. The method of solution of two-dimensional potential wave equations based on conformal mapping is applied to the simulation of wave behavior assigned by different initial conditions, defined by the Joint North Sea Wave Observation Project and Pierson–Moskowitz spectra. It is shown that nonlinear wave evolution sometimes results in the appearance of very big waves. There are no predictors for the appearance of extreme waves; however, the height of dimensional waves is proportional to the significant wave height. The initial generation of extreme waves can occur simply as a result of linear group effects, but in some cases the largest wave suddenly starts to grow. It is followed sometimes by a strong concentration of wave energy around a peak vertical. It takes place typically for one peak wave period. It happens to an individual wave in physical space, with no energy exchange with surrounding waves taking place. A probability function for steep waves has been constructed. Such type of function can be used for the development of operational forecast of freak waves based on a standard forecast provided by a three-dimensional generation wave prediction model (WAVEWATCH or wave modeling). © *2009 American Institute of Physics*.
[DOI: 10.1063/1.3175713]

## I. INTRODUCTION

Waves named "freak" or "rogue" are formally defined as waves whose height exceeds the significant wave height $H_s$ =2 (sometimes 2.1 or 2.2). So, if the significant wave height is equal to 1 m, then all waves with a trough-to-crest height exceeding 2 m should be referred to the category of freak waves. It is hard to imagine that such waves can be characterized as "monster" waves even for a small vessel. On the other side, if a steady West wind with a speed of 20 m/s in the South Ocean generates a wave with a height of around 20 m and a length of around 0.5 km (according to reports of oceanographers sailing in those areas, such waves are not rare), then such a wave would just lift and drop a vessel, the only damage incurred being yet another attack of seasickness among the vessel crew. According to marine folklore, freak waves appear as "walls of water" with "holes in the sea" around them. Quite naturally, no one would pay attention to the walls or holes of 1 m in height. It is assumed that such walls should be considerably higher than the elevation of the observer above the peak of an incoming wave. For a small yacht, a breaking wave with a trough-to-crest height of 4 m can appear as a freak wave. The same wave, however, seems to be just a usual steep wave for a skipper of a huge tanker. Such a wave is definitely dangerous and can be obviously called a monstrous wave by the inhabitants of the Lilliputian land.

Evidently, a current scientific definition of the term freak wave is imperfect. Remarkably, sea folklore provides a better description of freak wave properties, focusing on their shape and assuming, of course, that they are very big. The term "vertical walls" definitely indicates that the waves surge before an observer and undergo the active phase of breaking. Linear velocities of water in the breaking waves approach the phase speed of the waves, which for the developed sea is close to the wind speed. A vertical wall does not lift a vessel; it hits it. Such waves at wind of 40 m/s can develop a dynamic pressure of about $10^6$ Pa, which is too much even for a tanker. Obviously, the great energy releasing at breaking is not the only weapon carried by extreme waves. Another dangerous property of extreme waves is the high gradient of the slope or vertical acceleration: a big vessel can be broken on a wave of great curvature. Definitely, other properties are also important. Big and long though nonbreaking waves can be dangerous for sea platforms, while they are relatively safe for sea vessels.

So, the classification of dangerous waves must be different for different objects, floating or fixed, for deep sea or near-shore area, and it must consider not only the size of waves but also their shape and mechanical properties. Considering practical application of the rare wave theory, we can also come to the conclusion that a strict unconditional "definition" of freak waves is not required at all. For better use of the research recommendations, it would be more efficient to define categories of freak waves, as it has been done, for example, for tropical storms. A reasonable warning on the appearance of such waves should sound like as follows: from 6 a.m. today until 6 a.m. tomorrow in a specific area of $100 \times 100$ km$^2$ a breaking wave with a height of 10 m (category three) shall be one of $1000 \pm 200$ waves, a breaking

[a)]Telephone: +7-812-230-7293. Electronic mail: dmitry-chalikov@yandex.ru.

 

wave with a height of 15 m (category five) shall be one of $8000 \pm 1000$ waves, etc." For unbreaking waves the probability of such waves is somewhat higher. The probability of coming across a freak wave is convenient to express in terms of expectance time for waves of different categories. A set of the most important dynamic characteristics of such waves can be also provided. Potential customers can decide for themselves whether it is a real freak wave and modify either their route or degree of preparedness accordingly. Similar recommendations can be developed for ship designing, sea constructions, and insurance purposes. Naturally, extreme waves are a phenomenon which manifests itself in a direct contact with an object. Such cases can be relatively frequent in uncomfortable areas with high winds and low intensity of navigation (for example, in middle and high latitudes of the South Ocean) and therefore remain unnoticed. On the contrary, in the areas of recommended routes (southern Africa), even a single catastrophic event may create a freak wave of publications. If the probability of extreme waves could be connected with the more or less standard oceanographic characteristics (for example, data on wind and wave climate), the estimations of climatology of dangerous waves of different categories might be very useful for industry, navigation, ship design, and, of course, insurance purposes. The reliable data on direct registration of freak waves events are sketchy, and operational monitoring of extreme waves from satellites is the most important though perhaps not resolved problem.

Attempts to completely attribute generation of big waves to focusing of wave energy on a specific geometry of currents or topography or certain wind conditions cannot be taken seriously. Each of such mechanisms can increase the effect of wave growth, but it is unlikely that it plays an important role in general statistics (independent of a specific location) for open oceans. It is well known that the frequency of big wave occurrence greatly exceeds the values calculated with the use of plain extrapolation of regularities obtained on a basis of the linear theory. At present, the "scientific community" is coming to the opinion that the main role in the appearance of such a phenomenon is played by the strong nonlinearity of waves, which makes the process of freaking much more frequent than might be predicted on the basis of the linear theory. This statement is also true for other branches of geophysical fluid dynamics: for example, the probability of a very strong wind also greatly exceeds the estimations based on the Gaussian distribution. For insurance purposes, it would be a great mistake to do estimations of tornado probability with the use of Gaussian extrapolation of the wind speed climatic probability.

At present, freak waves are the subject of intense research. Various theoretical investigations and laboratory experiments were conducted over the recent years (see reviews in Refs. 1 and 2) As it usually happens at the beginning of studies, the generation of freak waves was explained by many different mechanisms. The linear theory is evidently unable to describe an extreme wave onset. That is why the linear theory additionally assumes the possibility of wave energy geometrical focusing on specific structures of surface currents or/and bathymetry. However, it is known that freak waves appear both in deep and shallow waters in the presence or absence of appropriate current systems. Besides, it is unlikely that the focusing can provide such fast development. All the processes mentioned above have been investigated within the framework of weakly nonlinear models, such as the nonlinear Schrödinger equation, the Davey–Stewartson system, the Korteweg–de Vries equation, and the Kadomtsev–Petviashvili equation. These approaches considerably simplify the principal equations, since they reduce them to a single equation for surface elevation. Recently, Janssen[3] explained the freak wave occurrence as a consequence of a four-wave interaction. His suggestion is based on Zakharov's equation,[4] which predicts deviation of the Gaussian process, resulting in nonzero kurtosis but still zero skewness. Real waves have always positive skewness. It is unlikely that the model that cannot simulate a simpler and more important third-order moment (skewness) is able to correctly simulate a much more complicated fourth-order moment. There also exists a hypothesis that a freak wave can arise due to the specific atmospheric forcing. This statement is evidently true. Homer[5] once noticed that "…it is the force of wind that makes the waves so great." However, time scales of wind forcing are too great to explain a sudden rise of one out of many waves. Wind forcing creates a high density of wave energy, but it is just a long prehistory of stochastic freaking process connected with the spontaneous transformation and release of huge amounts of energy. The Benjamin–Feir (BF) instability[6] (BFI) is an important mechanism of developing wave spectrum homogeneity due to the slow growth of new wave components; however, it is inapplicable for the finite-amplitude fast wave evolution controlled by conservation of energy and strong nonlinearity.[7] The similarity between BF instability criteria applicable to discrete spectrum and the so-called BFI index[5] introduced for a developed spectrum is doubtful.

The most popular tool for the investigation of nonlinear waves is the nonlinear Schrödinger equation. This equation has been playing an important role in the investigation of freak wave generation. Numerical calculations based on the Schrödinger equation show that some of freak wave cases can appear as a result of modulation instability and focusing of energy.[8–10] Using the Joint North Sea Wave Observation Project (JONSWAP) spectrum, Onorato *et al.*[11] performed numerical experiments to investigate freak wave generation and its statistics. In particular, it was shown that for a narrow spectrum (increased value of "enhancement" coefficient in the JONSWAP spectrum) the probability of rogue wave occurrence is increasing. However, the numerical approach based on the Schrödinger equation can be referred to as a qualitative method because the results of such simulation look strange sometimes: they make an impression that the waves simulated in this way seem unnaturally big. Some of the calculations (for example, Ref. 12) show that enhancement of amplitude can be seven times as high. The simulations based on equations of fluid dynamics show that big waves always tend to have strong asymmetry before breaking.[13,14] The simplest definition of asymmetry is the ratio of distance between forward trough and crest to distance between back trough and crest. This characteristic is most important as indicator of breaking onset. Breaking restricts growth of amplitude and makes statistics of big waves more natural. The evident advantage of numerical approach based on the Schrödinger equation is that it can be generalized for qualitative investigation of two-dimensional (2D) waves.[9] In numerical investigation of one-dimensional (1D) wave evolution the use of precise numerical models based on fluid mechanics equations[15–18] is evidently preferable.

It should be noted that the numerical schemes for three-dimensional (3D) potential equations have also been developed (see Refs. 19–21). A 3D exact model has been developed by the author of this paper (see the Appendix); however, as for all 3D fluid mechanics models, the calculations with this model are very expensive. The 3D model is more complicated than the 2D model, and it uses a significantly greater number of degrees of freedom than the 2D model does (currently, it employs about 10 000–100 000 modes). Such modeling requires huge computational resources (fast multiprocessor computers and long-term calculations), so the above approach can be applied only for simulation of single cases of 3D wave evolution. Freak waves are a rare phenomenon both in nature and in computer simulations. Performing a long-term run with a 3D model can give no results, as it most likely happens that a freak wave will not appear. Currently, it is difficult to use a 3D approach for a systematic investigation of the mechanics and statistics of freak waves in the same way as it is demonstrated below on the basis of the 2D equations. It is unlikely, that in the nearest future the 2D approach would be completely replaced by the 3D approach. However, the models for 3D wave simulations do already exist, and the progress in computer technology can overturn any pessimistic predictions of that kind.

At present, two different models use the principal 2D fully nonlinear equations for potential flow with a free surface: a numerical model based on a boundary integral developed by Dold and Peregrine,[15] described in detail by Dold,[16] and a model based on conformal mapping.[13,16,18] Actually, Dold's model was the first model for surface wave simulation based on fluid mechanics equations, opposite to numerous approaches using simplified, severely truncated, or crippled 1D equations (see references in Ref. 13 and more information in reviews in Refs. 1 and 22). It is interesting that the sophisticated numerical analysis was often used also for the solution of substitute 1D equations. It remains unclear what those efforts have been undertaken for, since the tiny initial 1D equations could be solved easily with the highest accuracy at least 25 years ago. Dold's approach[16] has been successfully used for the investigation of many problems including wave breaking.[23] However, later it was found that a simpler and more precise scheme could be constructed on the basis of conformal mapping. For the *stationary problem*, the mapping represents a classical complex variable method (see, e.g., Refs. 24 and 25), originally developed by Stokes.[26] For the stationary problem the method employs the velocity potential $\Phi$ and the stream function $\Psi$ as independent variables. In fact, the approach based on *nonstationary* conformal mapping had been formulated long before it was used for numerical integration. It had been introduced by Whitney[27] and by Ovsyannikov,[28] and later, it was considered in Refs. 29 and 30. Tanveer[31,32] used that approach for the investigation of the Rayleigh–Taylor instability and the generation of surface singularities. However, no authors of those works used conformal transformation for simulation of long-term multimode periodic wave dynamics. Such a 2D model was completed in 1992, when a systematic use of the new approach to different problems was initiated. A numerical scheme based on conformal mapping (and its validation) as well as the results of long-term simulations were presented at the ONR meeting held in Arizona in 1994. The scheme for arbitrary depth was described in detail by Chalikov and Sheinin.[17,18] More details for the case of shallow water were given in Ref. 33. Later, the method developed was used with some minor modifications in Refs. 34 and 35 to demonstrate certain nonlinear properties of steep waves.

The nonstationary conformal mapping for finite depth allows rewriting of the principal equations of potential flow with a free surface in a surface-following coordinate system. The Laplace equation retains its form, while the boundaries of the flow domain (i.e., the free surface and, in the case of finite depth, the bottom) are coordinate surfaces in the new coordinate system. Accordingly, the velocity potential in the entire domain receives a standard representation based on its Fourier expansion on the free surface. As a result, the hydrodynamic system of equations (not simplified) is represented by two simple evolutionary equations which can be solved numerically in a straightforward way and used for theoretical investigations. The assumption of potentiality simplifies the approach so significantly that the numerical scheme does not require any finite-difference approximations since the derivatives can be calculated precisely using the Fourier presentations, while nonlinearities can be approximated on a dense grid with a well estimated accuracy. For restricted order of nonlinearity this method is also precise and depends on the number of digits assigned for calculations. The model represents a rarity in geophysical fluid dynamics (though the potential one), when a real process can be simulated with nearly computer accuracy. This statement can be fully correct if surface steepness is not too high. Increase in local steepness often results in developing of instability and even overturning of sharp crests. Formally, conformal mapping exists up to the moment when an overturning volume of water touches the surface. In such an imaginary evolution, the number of Fourier modes required increases up to infinity. If some special measures (smoothing, see, for example, Ref. 16) are not taken, the calculations normally terminate much earlier due to strong crest instability,[36] shortly manifesting itself by separation of the falling volume into two phases. This phenomenon is obviously nonpotential. Hence, as in many branches of geophysical fluid dynamics, some special measures (which are arrogant from the point of view of potential theory) must be taken to prevent numerical instabilities at the same time considering the physical consequences of such events (e.g., conservation of volume, energy, and momentum).

Recently, the Chalikov and Sheinin (ChSh) model was used for the simulation of wave evolution at various initial conditions.[13] Numerical simulations of initially monochromatic waves with different steepnesses showed that the model was able to reproduce the onset of the breaking process when the surface becomes a multivalued function of the horizontal coordinate. An estimate of the initial critical wave height that divides nonbreaking and eventually breaking waves was obtained. Simulations of nonlinear evolution of a wave field were represented initially by two modes with close wave numbers (amplitude modulation) and a wave field with a phase modulation. Both runs result in the appearance of large and very steep waves; they also break if the initial amplitudes are large enough. The breaking process develops so quickly that the period of multivalued surface existence is quite short. Formally, the instability displays itself in the fast growth of high wave number modes, but physically, a tendency for separation of falling volumes is quickly developing, which makes it impossible to apply conformal mapping, potential approximation, and equations of fluid mechanics for single-phase fluid in general.

Next, the model was used for the simulation of nonbreaking evolution of wave fields with a great number of modes for many periods of the dominant wave.[37] The statistical characteristics of nonlinear wave fields for waves of different steepnesses were investigated including spectra, kurtosis and skewness, dispersion relation, and time scales, i.e., typical "lifetime" of waves. The mean values of kurtosis obtained in numerical experiments were close to 1, which was a result similar to that obtained in a wave tank,[38,39] while some values equaled 2 or even 3. The calculations showed that the presentation of a wave field as a superposition of linear waves is valid only for small amplitudes. Virtually, the high wave number components exchange energy with each other so quickly that it makes it impossible to even calculate their phase velocities. It was also shown that nonlinear wave fields are rather a superposition of Stokes waves, not linear waves. It is interesting to note that a moving wave surface composed of linear waves looks abnormally gentle, while a wave surface assembled from Stokes waves strikingly reminds images of the best animation cartoons.

Recently,[7] the model was used for numerical simulation of small-amplitude and finite-amplitude BF instability.[6,40] It was shown that the initially homogeneous train of Stokes waves undergoes several phases of evolution. Finally the wave field turns into a random superposition of nearly Stokes waves. If the initial steepness is large enough $(ak > 0.12)$, some waves become high, get asymmetric, and finally break. In the current work the initial conditions were assigned as a superposition of Stokes waves with preassigned initial spectrum and random amplitudes.

The work is considering simulation of numerous cases of nonlinear evolution of a 1D wave field, leading to breaking or/and to formation of extreme waves. The obtained results are used for preliminary estimations of occurrence, statistics, and some mechanical properties of extreme waves. It is shown below that extreme waves are a relatively rare but quite typical phenomenon which can be well simulated with the use of full fluid mechanics equations. The limitations of two dimensionality make the results less general than those which could be obtained with the use of the 3D model. However, it would be premature to start simulations using a highly complicated and expensive 3D model before trying all of the possibilities suggested by a fast and precise 2D model. Most in the scientific community hold an opinion that formation of freak waves (at least in its last stage) is mainly the 1D process, as the rate of strong nonlinear interactions between unidirectional waves is probably higher than for the directionally spread waves.[41] Hopefully, the effect of angular spreading will soon be investigated with the use of the 3D model (see the Appendix).

## II. EQUATIONS

Consider the periodic 1D deep-water waves, the dynamics of which is described by principal potential equations. Due to the periodicity condition, the conformal mapping for an infinite depth can be represented by the Fourier series (for details, see Refs. 17 and 18)

$$x = \xi + \sum_{-M \le k < M, k \ne 0} \eta_{-k}(\tau)\exp(k\zeta)\vartheta_k(\xi), \quad (1)$$

$$z = \zeta + \sum_{-M \le k < M, k \ne 0} \operatorname{sgn}(k)\,\eta_k(\tau)\exp(k\zeta)\vartheta_k(\xi), \quad (2)$$

where $x$ and $z$ are the Cartesian coordinates, $\xi$ and $\zeta$ are the conformal surface-following coordinates, $\tau$ is the time, $\eta_k$ are the coefficients of Fourier expansion of the free surface $\eta(\xi,\tau)$ with respect to the new horizontal coordinate $\xi$:

$$\eta(\xi,\tau) = h(x(\xi,\zeta=0,\tau),t=\tau) = \sum_{-M \le k \le M} \eta_k(\tau)\vartheta_k(\xi), \quad (3)$$

$\vartheta_k$ denotes the functions,

$$\vartheta_k(\xi) = \begin{cases} \cos k\xi, & k \ge 0, \\ \sin k\xi, & k < 0, \end{cases} \quad (4)$$

and $M$ is the truncation number.

Nontraditional presentation of the Fourier transform with definition (4) is, in fact, more convenient for calculations with real numbers, as $(\vartheta_k)_\xi = k\vartheta_{-k}$ and $\Sigma(A_k\vartheta_k)_\xi = -\Sigma kA_{-k}\vartheta_k$.

Note that the definition of both coordinates $\xi$ and $\zeta$ is based on Fourier coefficients for surface elevation. It follows then from Eqs. (1) and (2) that the time derivatives $z_\tau$ and $x_\tau$ for Fourier components are connected by the simple relation

$$(x_\tau)_k = \begin{cases} -(z_\tau)_{-k}, & k > 0, \\ (z_\tau)_k, & k < 0. \end{cases} \quad (5)$$

Due to conformity, the Laplace equation retains its form in $(\xi,\zeta)$ coordinates. It is shown in Refs. 17 and 18 that potential wave equations can be represented in the new coordinates as follows:

$$\Phi_{\xi\xi} + \Phi_{\zeta\zeta} = 0, \quad (6)$$

$$z_\tau = x_\xi \xi_\tau + z_\xi \varsigma_\tau, \quad (7)$$

$$\Phi_\tau = F\Phi_\xi - \tfrac{1}{2}J^{-1}(\Phi_\xi^2 - \Phi_\zeta^2) - z, \quad (8)$$

where Eqs. (7) and (8) are written for the surface $\zeta=0$ [so that $z=\eta$, as represented by expansion (1)], $J$ is the Jacobian of the transformation

$$J = x_\xi^2 + z_\xi^2 = x_\zeta^2 + z_\zeta^2, \quad (9)$$

and $\xi_\tau$ and $\varsigma_\tau$ are connected through the relation

$$\zeta_\tau = (J^{-1}\Phi_\zeta)_{\zeta=0}. \tag{10}$$

Equations (6)–(8) are written in a nondimensional form with the following scales: length $L$, where $2\pi L$ is a dimensional period in the horizontal, time $L^{1/2}g^{-1/2}$, and velocity potential $L^{3/2}g^{-1/2}$ ($g$ is the acceleration of gravity). Capillarity and external pressure were not taken into account in this investigation.

The boundary condition assumes vanishing of vertical velocity in depth,

$$\Phi_\zeta(\xi, \zeta \to -\infty, \tau) = 0. \tag{11}$$

The solution of the Laplace equation (6) with the boundary condition (11) yields to Fourier expansion, which reduces the system (6)–(8) to a 1D problem:

$$\Phi = \sum_{-M \le k \le M} \phi_k(\tau)\exp(k\zeta)\vartheta_k(\xi), \tag{12}$$

where $\phi_k$ are Fourier coefficients of the surface potential $\Phi(\xi, \zeta=0, \tau)$. Equations (6)–(8) and (10) constitute a closed system of prognostic equations for the surface functions $z(\xi, \zeta=0, \tau) = \eta(\xi, \tau)$ and the surface velocity potential $\Phi(\xi, \zeta=0, \tau)$.

For time integration, the fourth-order Runge–Kutta scheme was used. The choice of time step was done empirically. For example, for $M=100$, the time step $\Delta\tau$ was equal to 0.01. For $M=1000$, it was 0.002. Increase in local steepness and surface curvature sometimes forces application of smaller time steps.

The specific problem is that initial data are normally given in the Cartesian coordinates. They need to be converted into the $(\xi, \zeta)$ coordinates. For that purpose and for postprocessing of the results, an interpolating algorithm based on the periodic high-order spline functions has been developed. The algorithm carries out the transformation with high accuracy.

The problem of validation of the numerical scheme was discussed in Refs. 13 and 37. The scheme turned out to be very precise. The typical accuracy of solution for a sufficiently high resolution is $10^{-10}$. It is not surprising because the equations written in conformal coordinates become 1D evolutionary equations, which can be accurately solved by the Fourier-transform method without use of any local approximation. High accuracy of solution and preservation of integral invariants are crucial in numerical wave simulation, as the ratio of time scale for waves and time scale for energy input and dissipation is an order of $10^{-4}$, so wave motion is highly conservative, and at time scales of the order of period of waves it is practically adiabatic. Exactness of model is especially important for simulations of freak waves as the appearance of such a wave can occur after hundreds of periods of evolution. Our scheme meets such requirements. Propagation of very steep Stokes waves ($ak=0.42$) was simulated in Ref. 37 over 2 686 500 time steps (932 periods). The total energy for the number of modes $M=1000$ decreased only by $(3\times 10^{-8})\%$. The same calculations for $ak=0.42$ performed in Ref. 16 quickly collapsed due to numerical instability. The exact phase velocity of Stokes waves with $ak=0.42$, obtained for the stationary solution, is 1.089 578. A direct calculation of phase velocity of simulated Stokes wave gave the value of $1.089\,579 \pm 10^{-6}$. Note that validation of the model based on simulation of exact Stokes waves assigned in initial conditions is full and not trivial. The same procedures were performed for stationary analytical solution for capillary waves[25] and for gravity-capillary waves with different capillarities. Algorithms for generation of all the types of stationary waves, as well as validation of the nonstationary model, were described in Refs. 17 and 18 (see also Ref. 7). All those experiments have confirmed the highest accuracy of the scheme based on conformal transformation.

The adiabatic version of equations of wave theory (not necessarily potential) has a very important property of *self-similarity*: a nondimensional form of equations (outside of capillary range) does not include a nondimensional parameter. It means that just by simple scale transformation, the numerical results can be used for the analysis of gravity waves of any scale for the same nondimensional initial conditions. Hence, the breaking freak waves are exactly the same phenomenon as even the smallest breaking gravity waves. That is why the term freak waves can be used only for dimensional waves. The existence of input energy from the wind does not change this situation due to the large gap between time scales for the input and the fast local growth of separate waves (freaking). Note that self-similarity of the equation simplifies the investigation of wave dynamics, since the solution depends on initial conditions only, and each single run with nondimensional equations corresponds to an infinite number of real cases.

## III. DESCRIPTION OF NUMERICAL EXPERIMENTS

In this study the method of approximation of wave surface by superposition of Stokes waves developed in Ref. 7 was used. Briefly, the method is based on the use of "upper conformal coordinates" $(\xi_u, \zeta_u)$, similar to Eqs. (1) and (2) but written for domain $z > \eta$. It was shown that the superposition of linear waves assigned in this coordinate system after interpolation to Cartesian coordinates turns into superposition of Stokes waves with high accuracy. Note that full equations at any reasonable initial conditions after some accommodation period reproduce this effect too, since harmonic waves tend to turn into Stokes-like waves. In this paper initial generation of Stokes waves was done to accelerate transition to the statistically homogeneous regime.

In this study, we have applied the above described method for numerical simulation of surface waves for the investigation of evolution of a wave train assigned by the 1D version of the JONSWAP spectrum $S_f$ for finite fetches as a function of frequency $\omega$,

$$S_f(\omega) = \frac{\alpha g^2}{\omega^5}\exp\left[-\beta_1\left(\frac{\omega_p}{\omega}\right)^4\right]\gamma^r, \tag{13}$$

where $\beta_1 = 1,25$, $\gamma=3.3$, and $\omega_p$ is a parameter whose value is close to the frequency of the spectral peak $S_p$. Other parameters can be expressed through $\omega_p$:

$$r = \exp\left(-\frac{(\omega-\omega_p)^2}{2\sigma^2\omega_p^2}\right),$$

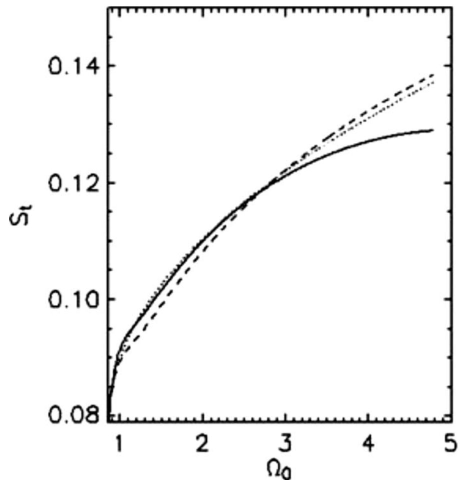


FIG. 1. Dependence of steepness parameter $S_t$ on wave age $\Omega_0 = U_{10}/c_p$. Solid line corresponds to the calculation with a combined JONSWAP/PM spectrum [Eq. (15)] with $\gamma=3.3$, dashed line corresponds to the same spectrum but with $\gamma$ defined by Eq. (17), and dotted line corresponds to approximation (23).

$$\alpha=0.0099\Omega 0.66,$$

$$\sigma = \begin{cases} 0.07, & \omega \le \omega_p, \\ 0.09, & \omega > \omega_p, \end{cases}$$

where $\Omega = \omega_p U_{10}/g = U_{10}/c_p$ is the nondimensional frequency in a spectral peak and $c_p$ is the phase velocity.

It is well known that approximation (13) overestimates the spectrum at low values of nondimensional frequencies $\Omega \le 1.3$ (large fetches). To keep the right asymptotic behavior, the approximation (13) was combined with the Pierson and Moskowitz (PM) spectrum for fully developed waves,

$$S_\infty(\omega) = \frac{\alpha g^2}{\omega^5}\exp\left[-\beta_2\left(\frac{\omega_0}{\omega}\right)^4\right], \tag{14}$$

by the following relation:

$$S = S_\infty W + S_f(1-W), \tag{15}$$

where $W$ is the weight, which is convenient to represent as a function of $\Omega$. It is easy to calculate that $\Omega_\infty = 0.855$ for the PM spectrum. Since transition from spectrum $S_\infty$ to $S_f$ happens in a small interval of $\Omega$, a function $W$ quickly decays with growth of the distance $\Omega - \Omega_\infty$. The function $W(\Omega)$ was approximated by the formula

$$W = \exp[-15(\Omega - \Omega_\infty)]. \tag{16}$$

In the initial JONSWAP approximation the enhancement parameter for spectrum $\gamma$ was accepted as constant: $\gamma=3.3$. Later, some investigators came to the conclusion that this parameter can be a function of a fetch or peak frequency $\omega_p$. According to Ref. 42, $\gamma$ increases with $\Omega$ as

$$\gamma = 1.224\Omega. \tag{17}$$

Merging was made in a very narrow interval [0.855–1] (see Fig. 1). The number of cases falling in this interval is so small that it does not influence the statistics. Approximations (13) and (14) were rewritten in terms of wave numbers using a dispersion relation, which is valid at least up to $3\Omega_p$ (see Ref. 37). The nondimensional wave number $k_p$ in a spectral peak is a parameter of initial conditions. To describe the low wave number slope of the spectrum, $k_p$ should be larger than 1, and for a good approximation of the entire spectrum (and its spreading due to nonlinearity) $k_p$ should be considerably smaller than the total number of modes, $M$. Actually, $k_p$ is a parameter of accuracy of approximation. Initial conditions for Fourier coefficients of free surface $\eta(x)$ were assigned in the form

$$\begin{aligned} |h_k| &= (2S(k)\Delta k)^{1/2}, \\ \eta_k &= |h_k|\sin(\varphi), \\ \eta_{-k} &= |h_k|\cos(\varphi), \\ k &= 1,2,3,\ldots,k_m, \end{aligned} \tag{18}$$

where $|h_k|$ is the amplitude of the $k$th mode, $\eta_k$ and $\eta_{-k}$ are the Fourier coefficients in the Cartesian coordinates, and $\varphi$ is the random (over $k$ and over different runs) phases of modes uniformly distributed in the interval $(0-2\pi)$. The Fourier coefficients $f_k$ for surface potential $f(x)$ were assigned by

$$f_k = -|k|^{1/2}a_{-k}, \quad k=-M_i,M_i, \tag{19}$$

where $M_i$ is the number of modes assigned in the initial conditions. After inverse Fourier transforming, functions $\eta(x)$ and $f(x)$ were transferred from the upper coordinates $(\xi_u,\zeta_u)$ to the "lower coordinates" [Eqs. (1) and (2)] by periodic spline interpolation, providing accuracy of the order of $10^{-11}$ for very steep waves and $10^{-30}$ for medium amplitude waves. Postprocessing was done for data transferred back to the Cartesian coordinate by the same algorithm. A peak of spectrum was placed at $k_p=8$ and $\Omega=\sqrt{k}=2.83$ or at $k_p=20$ and $\Omega=4.47$. A number of waves assigned in initial conditions $k_m$ was equal to 32, so the amplitude of the smallest assigned wave was at $4^3$ smaller than the amplitude $h_p$ in the peak of the spectrum.

The spectral tail was developing during the first period of the peak wave at higher frequencies. This evolution occurs for any steepness. Simulation of the wave evolution assigned by Eqs. (13)–(17) was performed for the number of modes $M=2000$ and the number of grid points $N=8000$, which provided sufficient resolution both in the Fourier and physical spaces. The control runs with resolution $M=4000$ and $N=16\,000$ revealed the same statistical properties of the solution. The time step $\Delta\tau$ was equal to 0.002 (and 0.001 for $M=4000$). Application of a twice-shorter time step for strongly nonlinear cases proves that differences between results are negligible, excluding small variations at the last time steps before breaking. Many runs were terminated due to some wave tendency for overturning. Several dozens of runs for a relatively small steepness lasted up to 2000 periods with no breaking event. A criterion for terminating a run was defined by the first appearance of a nonsingle value of surface $\eta$:

$$x(i+1) < x(i), \quad i = 1,2,3, \dots ,N-1. \tag{20}$$

The integration was possible to continue shortly after that moment (see Ref. 13), but the details of this development are not a subject of this paper. It is important to emphasize that after the moment when the criterion (20) has been reached, the solution never returns to stability: the volume of fluid crossing the vertical $x(i)$ quickly increases. Up to this moment conservation of the sum of potential and kinetic energies, horizontal momentum, and volume was excellent. When a surface becomes a nonsingle value (at the initial stage of breaking), conservation of invariants still holds, but later, a sharp increase in energy occurs, and a further integration becomes useless. Usually it happens just for one Runge–Kutta time step, so probably, a primary cause of the numerical instability is the growth of the right side of Eqs. (6)–(8). Disintegration of the solution happens mostly due to inapplicability of potential approximation and, generally, fluid dynamic equations for a single-phase fluid.

Extreme waves are a rare phenomenon in nature. Therefore, they are reproduced rarely in the numerical simulations too. Statistical characteristics of a wave field, as well as probability of extreme waves, seem to depend on inverse wave age $\Omega$ and on the initial set of phases, especially for young steep waves. The dependence on the preassigned set of phases can be excluded by repeated calculations for the same set of amplitudes with a random choice of phases. One cycle of calculations includes 60–90 cases for different peak frequencies:

$$\Omega_n = \Omega_\infty + 0.0294n, \quad n = 1,2,3, \dots ,60-90, \tag{21}$$

where $n$ is the number of runs in one cycle and $\Omega_\infty=0.855$ is the nondimensional peak frequency for the PM spectrum. The upper limit of $\Omega$ was equal to 3.50, which corresponded to the young sea. That cycle was repeated 64 times. Cycles 1–48 were performed with the use of a fixed enhancement parameter $\gamma=3.3$ and a peak wave number $k_p=8$, while cycles 49–64 were performed when $\gamma$ was assigned by formula (17) and $k_p=20$. The total number of runs was equal to 4294. The calculations performed in a Dell workstation (speed is 3.1 MHz) took about 3 months. To trace the generation and evolution of extreme waves, wave profiles, containing the waves with a trough-to-crest height greater than $2H_s$, were recorded. Many statistical characteristics, including different moments, were calculated in the course of simulations. The total volume of data selected and recorded was around 100 Gbits.

The parameter $\Omega=U_{10}/c_p$ (or nondimensional fetch) is convenient for the calculation of the explicit form of the wave spectrum. However, the use of $\Omega$ in operational analysis of wave spectra (measured or calculated by a wave forecasting model) is not convenient, as a wave spectrum can be a nonsingle-peak spectrum or it can be blurred with a swell, the energy of which might be comparable to the energy of wind waves, produced by a local wind. If a swell is strong, its interaction (for example, through Benjamin–Feir–McLean instability) with the locally produced wind waves can result in the generation of extreme waves. That is why we introduce more robust characteristics, expressed as a product of significant wave height $H_s$ and wave number $k_s$ weighted by the spectrum

$$S_t = k_s H_s, \quad \text{where } H_s = 4\sqrt{S} \quad \text{and} \quad k_s = \frac{\Sigma_0^M k S_k}{\Sigma_o^M S_k}. \tag{22}$$

For the JONSWAP-PM spectrum [Eq. (15)] the dependence of $S_t$ on $\Omega$ is monotonic (Fig. 1). This function for parameter $\gamma$ defined by Eq. (17) is approximated by the following relation:

$$S_t = S_0 + A_0(\Omega - \Omega_0)^{1/2}, \tag{23}$$

where $S_0=0.316$, $\Omega_0=0.855$, and $A_0=0.118$ (dotted line). Point $\Omega_0$ corresponds to the PM spectrum for a developed sea. Parameter $S_t$ characterizes the nondimensional density of wave energy. For young waves the parameter $S_t$ is larger than for old waves, because the energy is concentrated in small wavelengths (large wave numbers).

## IV. BREAKING AND SURVIVING EXTREME WAVES

For practical needs consideration of height of a wave crest above a mean level $z=0$ does not make any sense, because wave power depends on the overall wave height from its trough to the crest. It is not easy to detect this height formally. The calculation of a vertical distance between the maximum and its nearest minimum does not give the right answer, because there can be some local extremes there; hence, the wave height might be underestimated. Obviously, the extreme wave must be found between large waves. That is why the height of extreme waves $H_{tc}$ in each record $\eta(x)$ was defined here as the difference between the absolute maximum and absolute minimum in a moving window of length $L_e$. It would be reasonable to define $L_e=1.5L_P$, where $L_p$ is the length of the wave in the peak of the spectrum, $L_p=2\pi/k_p$, and $k_p$ is the actual wave number in the spectral peak. The extreme waves with a length exceeding $1.5L_p$ were practically absent. It will be demonstrated below that the development of freak waves happens very quickly—normally within one or a couple of wave periods. Let us define a unit event as a run of a wave over its single period. This suggestion allows us to estimate the total number of events used for statistical processing as equal to about $15 \times 10^6$. In this paper, the main attention will be focused on statistical properties of a nondimensional trough-to-crest wave height $H_f=H_e/H_s$.

If extreme waves were always breaking, a number of such waves would be close to the number of runs (there are a few cases when a run reached the designated end without breaking). In fact, the recorded ensemble of large waves was much greater, since the development of extreme waves was not always interrupted by breaking. This conclusion is opposite to results obtained in Ref. 43, where it was concluded that all freak waves are breaking waves. Many of the waves return to medium sizes again after they have gone through intense enhancement. The probability distribution for breaking and nonbreaking waves (normalized by total number of waves) is shown in Fig. 2 by dashed and solid lines, respectively. The fast decrease in probability for small $H_f$ simply

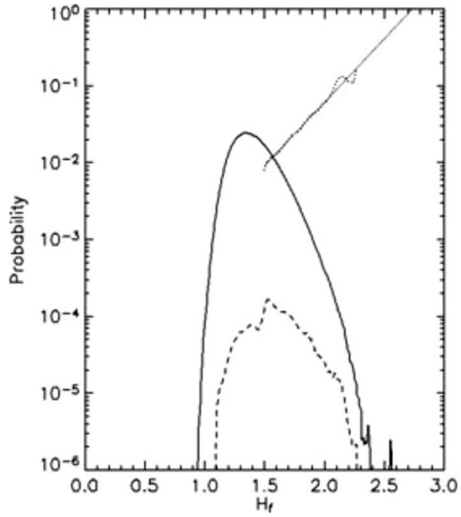


FIG. 2. Distribution of probability of trough-to-crest height $H_f$ for breaking (dashed line) and nonbreaking (solid line) waves defined with the use of window length $1.5L_p$. Dotted line is the ratio of the number of breaking waves and the number of nonbreaking waves; thin line represents approximation (24).

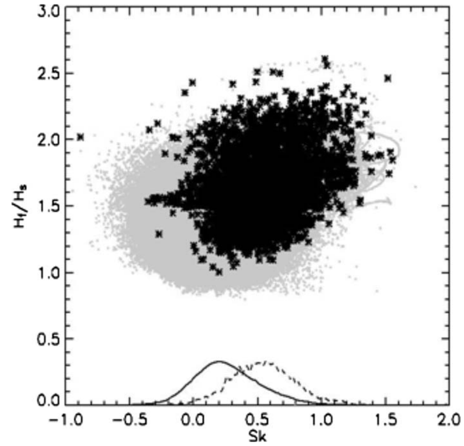


FIG. 3. Dependence of extreme wave height $H_f$ on parameter $S_t$ [Eq. (22)]. Aggregated gray dots correspond to nonbreaking waves (1 637 316 cases), while asterisks correspond to breaking waves (4742 cases). Solid line represents distribution of the number of cases for nonbreaking waves, and dashed line shows the same distribution for breaking waves, both of them normalized by the corresponding number of events.

shows that there were no small waves in the selected window, but the decrease in probability for large $H_f$ reflects rarity of freak waves. The estimation of probability for a smaller window (up to $0.5L_p$) showed that even short waves can break; however, this phenomenon is outside the scope of the subject covered by the current paper. The ratio of the total number of nonbreaking waves to that of breaking waves $R_{nb}$ (showed by dotted curve in Fig. 2 equals to 140 for the selected window. However, for each wave height this ratio $r_{nb}(H_f)$ is different: for freak waves $H_f>2$ the ratio $r_{nb}$ approaches 10. The exponential extrapolation of $r_{nb}$ (thin line),

$$r_{nb} = 10^{-4.51+1.65H_f}, \tag{24}$$

to high values of $H_f$ shows that all of the waves exceeding $H_f=2.7$ do break. This tendency looks reasonable, though the critical value of $H_f$ cannot be considered as well estimated.

It would be very useful to find connection between the trough-to-crest wave height and certain integral properties of a wave field. For these purposes, we plot the value of the biggest trough-to-crest height defined for every record of the surface against integral characteristics of a wave field calculated for the same wave profile. The dependence of the biggest trough-to-crest wave height on statistical characteristics calculated over the entire instantaneous wave profile is given in Figs. 3–5. In Fig. 3 the dependence of the largest trough-to-crest wave on parameter $S_t$ is given. The parameter $S_t$ characterizes wave age and in general the density of the potential energy. Note that the parameter $S_t$ is not invariant, but being a low-order moment, it remains relatively stable.

One could expect that a high energy wave field, characteristic of young waves and strong nonlinearity, can generate nondimensional large waves (normalized by $H_s$) more frequently than the waves of low energy and weak nonlinearity. However, as can be seen from Fig. 3, such suggestion proves to be incorrect: large waves have rather a tendency to appear in the old wave field with low steepness. It becomes even more evident for freak waves ($H_f \geq 2$) which are generated according to our data only in a developed wave field ($U_{10}/c_p \equiv \Omega < 1.4$). The tendency for increase in freak wave population with decrease in $S_t$ is well traced for cases of breaking waves (indicated by asterisks in Fig. 3). However, it can be seen that some of the freak waves (gray dots in the upper part of the panel) do not break at all.

Thus, nonlinearity seems to be working opposite to what was expected. It is a paradox, but this result can be still explained by the influence of nonlinearity. If a wave-wave interaction is quite energetic, the waves come to a breaking

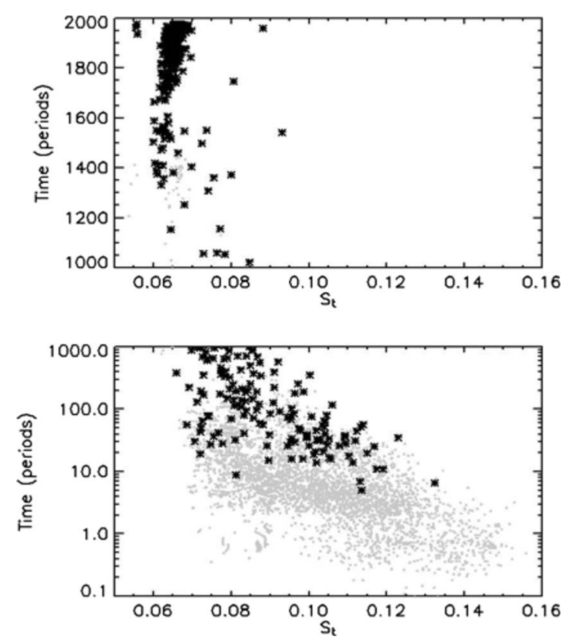


FIG. 4. Time of wave evolution up to onset of breaking (expressed in peak wave periods) vs parameter $S_t$ [Eq. (22)]. In the upper panel a linear scale for time is used, while in the bottom panel a logarithmic scale is used. Gray dots correspond to the case when values of $H_f$ before breaking were less than $H_f=2$, and asterisks represent the cases with $H_f>2$.

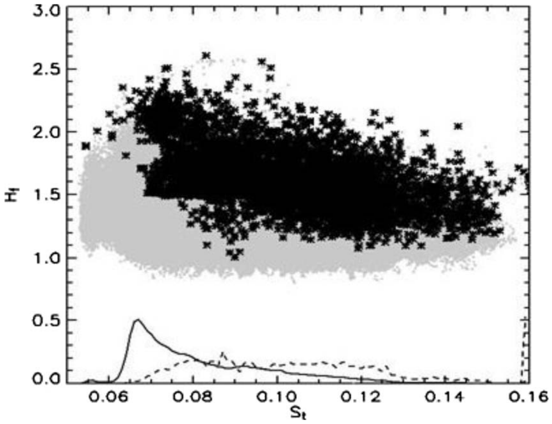


FIG. 5. Extreme wave height $H_f$ vs skewness Sk. Gray point, black asterisks, and lines are the same as in Fig. 3. The number of points is the same as in Fig. 3.

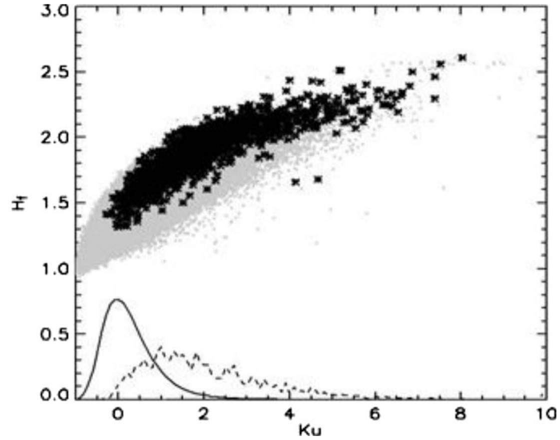


FIG. 6. The same as in Fig. 5 but for kurtosis Ku The plot includes 501 365 cases of unbreaking waves and 1165 cases of breaking waves.

point earlier than in the case of weak interactions, before the process of freaking (considered below) takes place. This effect is clearly demonstrated in Fig. 4, where the time period up to the breaking point is plotted against parameter $S_t$ characterizing the degree of nonlinearity. The waves with $H_f > 2$ are indicated in the plot by asterisks and all other waves by gray dots. As seen, large waves appear mostly in a wave field with low steepness, and steep waves rarely exceed the value $H_f=2$. To express it in metaphorical terms, active waves become *jealous* of the excessive growth of their neighbors.

Investigation of the connection of extreme wave probability with integral characteristics was continued for high-order moments: skewness Sk and kurtosis Ku, defined as

$$\bar{\eta} = \frac{1}{N}\sum_{j=0}^{N} \eta_j,$$

$$V = \frac{1}{N-1}\sum_{j=0}^{N} (\eta_j - \bar{\eta})^2,$$

$$\mathrm{Sk} = \frac{1}{N}\sum_{j=0}^{N} \left(\frac{\eta_j - \bar{\eta}}{\sqrt{V}}\right)^3, \tag{25}$$

$$\mathrm{Ku} = \frac{1}{N}\sum_{j=0}^{N-1} \left(\frac{\eta_j - \bar{\eta}}{\sqrt{V}}\right)^4 - 3,$$

where summation is performed over all the knots in the calculated wave profile transferred to the Cartesian coordinates. The maximum values of the trough-to-crest height in a single record $H_f$ are plotted in Fig. 5 against skewness Sk, calculated over this record. Skewness reflects a vertical asymmetry of disturbances. As seen, the skewness values considerably exceed zero. It indicates that the wave field is closer to superposition of sharp-crested modes than to that of linear waves.[37] In fact, a skewness value of wave profiles corresponding to the events of breaking is somewhat higher than that for nonbreaking cases. The asterisks are shifted up compared to gray dots, and the maximum of probability for breaking cases (dotted line) is shifted to higher values of skewness for nonbreaking cases. However, there is no evident connection between the height of extreme waves and their corresponding skewness.

It is remarkable that the connection of $H_f$ with kurtosis Ku (Fig. 6) looks better pronounced: the growth of $H_f$ is distinctly succeeded by higher values of Ku both for breaking and unbreaking waves. The number of cases included in Fig. 6 is smaller than for Figs. 3 and 5 as recording of Ku was implemented, starting from case 49. This connection seems to have confirmed Janssen's hypothesis[3] that a kurtosis can serve as a *predictor* for freak waves. To clarify the nature of this dependence, cross-correlation functions $R_t$ between variables Ku and $H_f$ were calculated for 288 randomly chosen (and long enough) runs (Fig. 7). The time lag $\Delta t$ is expressed in peak wave periods. As seen, simultaneous values of Ku and $H_f$ are well correlated at $\Delta t=0$ (where $R_t=0.7-0.8$), though the correlation quickly decreases with growing $\Delta t$. At $\Delta t \cong 10-20$ peak wave periods the correlation becomes insignificant. For a real large wave with the

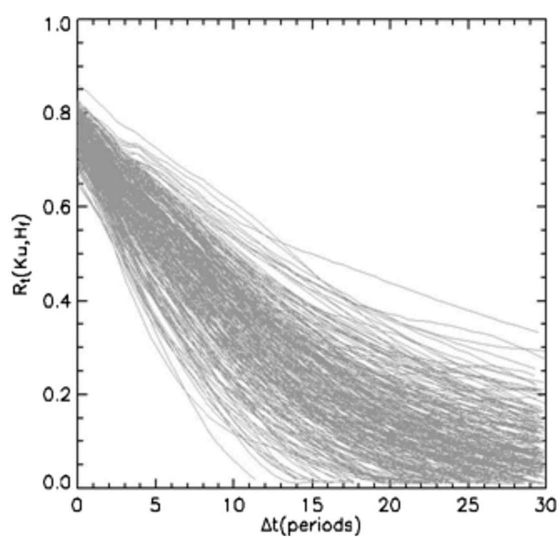


FIG. 7. Cross-correlation functions $R_t(\mathrm{Ku},H_f)$ for kurtosis Ku and extreme trough-to-crest wave heights $H_f$ calculated for 288 randomly chosen runs. Lag time is expressed in periods of peak wave.

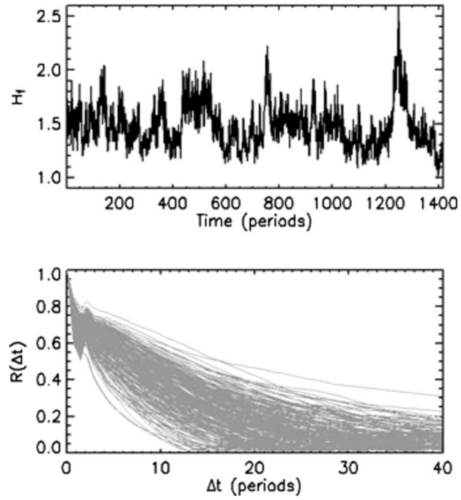

FIG. 8. Top panel is an example of extreme wave height $H_f$ evolution, while the bottom panel represents the autocorrelation function calculated for the cases of Fig. 7.

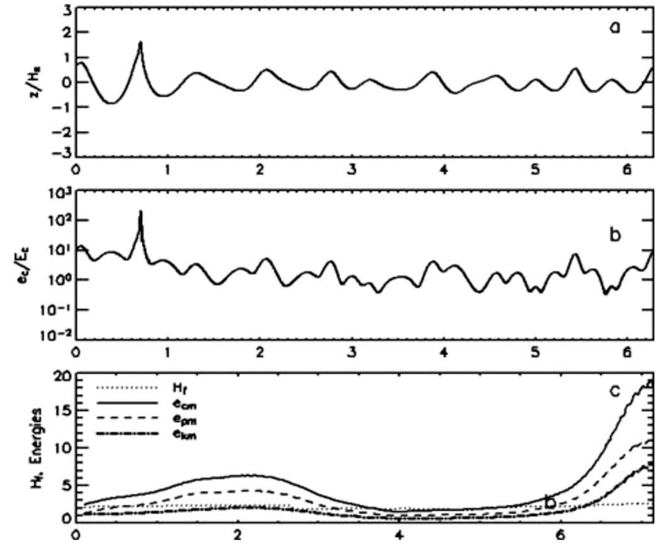

FIG. 9. Nondimensional columnar energy $k_p e_c / H_s^2$ vs trough-to-crest height of extreme waves. (a) Example of a wave surface containing a freak wave with $H_f$=2.5 before its breaking; (b) a profile of total columnar energy normalized by the averaged columnar energy [in panels (a) and (b) abscissa corresponds to the horizontal distance]; (c) a temporal evolution of extreme wave heights $H_f$ and maximum values of $e_{km}$, potential $e_{pm}$, and total $e_{cm}$ columnar energies prior to breaking. Abscissa corresponds to time.

period of the order of 20 s this time is equal to 6 min. Hence, a kurtosis and an extreme wave are interconnected at distances up to several hundred meters. The experiments described in Ref. 41 have proved that kurtosis is a good indicator of big wave appearance in a wave tunnel.

It means that kurtosis cannot serve as a predictor for practical applications but it is rather an *indicator* of local conditions. It is not surprising, as both high kurtosis and presence of large wave(s) reflect the same geometrical properties of a wave profile: sharpness and heights of crests. The explanation of this effect is quite simple: since the moment has fourth order, the contribution of high elevation is big. For the sixth, eighth, and any higher even moments the connection should be closer, Note that our conclusion is obtained with the use of relatively short wave profiles, containing 10–20 peak waves, so that the weight of the extreme wave turns out to be comparatively high. Consequently, the connection of kurtosis and extreme wave height is overestimated in our example. For far larger wave ensembles, an impact of rare extreme waves on the values of kurtosis evidently becomes negligibly small. It completely eliminates any possibility of using kurtosis not only as a predictor but also as an indicator of freak waves. The wave spectrum predicted by wave forecasting models reflects conditions averaged over an elementary cell of a numerical scheme. The cell can include many thousands of waves. Just several of them during very short periods of freaking can get very large. It is known that high-order moments are very sensitive to perturbations. Definitely, any calculations of the fourth-order moment on the basis of the averaged wave spectrum, predicted with low accuracy, are quite impossible.

An example of extreme wave evolution is given in Fig. 8 (top panel). Each value of $H_f$ is defined for a single record including 18–22 peak waves. The time interval $\Delta t$ between records was equal to 0.71 peak wave period. It can be seen that high values of $H_f$ appear sporadically, and the life of such a wave was very short. To illustrate this statement, autocorrelation functions $R(\Delta t)$ for cases of Fig. 7 are plotted in the bottom panel. As seen, $R$ decreases quickly with lag increase, and throughout dozens of periods the correlation becomes insignificant. The time scale of the correlation $T_R = \int_0^T R dt$ ($T$ is a period, long enough for accuracy of estimation), averaged for all 288 cases, equals to 5.5 periods of wave peak. Note that the run of Fig. 8 reproduces the largest extreme waves ($H_f$=2.59 at $t$=1250) ever recorded in our numerical experiments.

## V. THE PROPERTIES OF EXTREME WAVES

Densities of potential $E_p$ and kinetic $E_k$ energies averaged over $x$ (or $\xi$) can be calculated by the formulas

$$E_p = (2\pi)^{-1} \int_0^{2\pi} z^2 x_\xi d\xi,$$

$$E_k = (2\pi)^{-1} \int_0^{2\pi} \varphi \varphi_\zeta d\xi, \qquad (26)$$

$$E_c = E_p + E_k.$$

Energy of unit water column $e_c$ was calculated by the formulas, derived in conformal coordinates,

$$e_p = \frac{1}{2} z^2, \quad e_k = \frac{1}{2} \int_{-\infty}^{0} (\Phi_\xi^2 + \Phi_\zeta^2) J^{-1} d\zeta, \quad e_c = e_p + e_k, \qquad (27)$$

where the integral over depth was calculated with high accuracy in a stretched vertical grid, assuming that $\Delta\zeta_{j+1} = \varepsilon \Delta\zeta_j$, where $j$ grows down and the stretching parameter $\varepsilon$ equals to 1.10. A typical wave profile including freak wave with $H_f$ =2.5 at $x$=0.7 is given in Fig. 9(a). The corresponding profile of the overall columnar energy normalized by $E_c$ is given

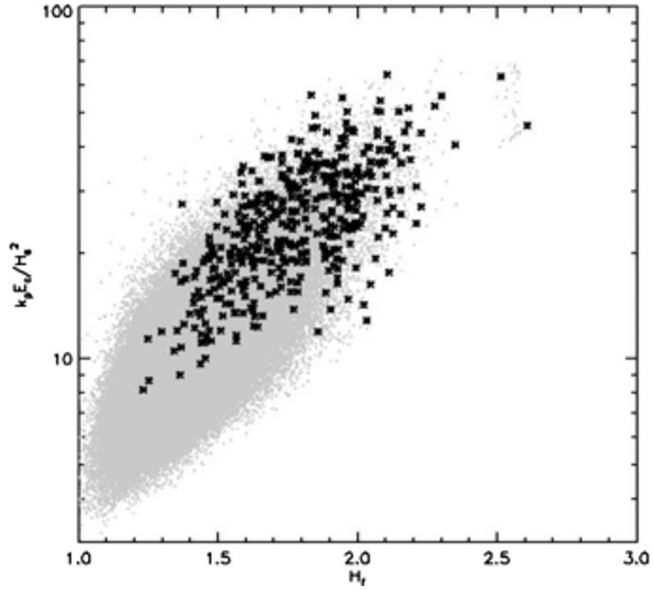


FIG. 10. Nondimensional columnar energy $k_p e_c / H_s^2$ vs trough-to-crest height of extreme waves.

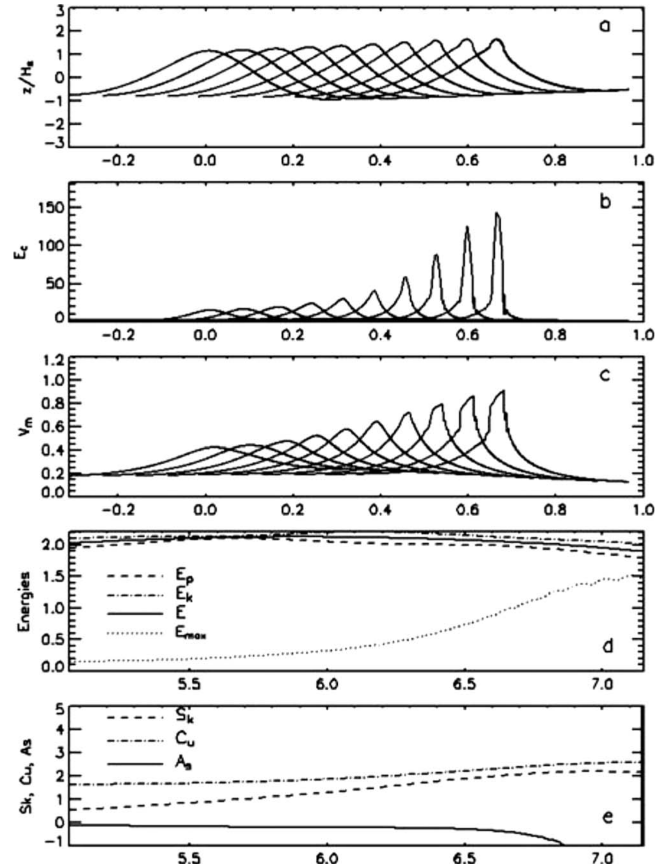


FIG. 11. Example of a run for $U_{10}/c_p=1.6$ ($S_t=0.105$). In panels (a)–(c) the horizontal axis is the distance: panel (a) represents successive profiles (separated by interval $\Delta t=0.02$) of the largest wave within the time range from $t=5.06$ ($H_f=2.10$ at $t=2.28$ periods) up to the overturning moment at $t=7.15$ (3.22 periods); (b) corresponds to (a) evolution of columnar energy $e_c$; (c) corresponds to (a) evolution of the absolute value of surface velocity normalized by phase velocity of peak wave $V_m$. In panels (d) and (e) the horizontal axis corresponds to time: (d) shows temporal evolution of maximum values of total $E_m$, columnar kinetic ($E_k$), potential ($E_k$), and total ($E$) energies; (e) represents temporal evolution of skewness (Sk), kurtosis (0.1Ku), and asymmetry (0.1As).

Fig. 9(b). The difference between the energies of usual waves and freak waves is so great that we had to plot energy $E=e_c/E_t$ in logarithmic scale. The energy at the peak of a freak wave exceeds the averaged energy $E_t$ by 150 times! It happens due to the concentration of energy in the vicinity of a freak wave crest. The evolution of the normalized trough-to-crest height $H_f$ of the largest wave for period (0–7.1) is shown in Fig. 9(c). As seen, an extreme wave height was increasing from $H_f=2.1$ to $H_f=2.5$ over this period, but its energy has grown up to ten times of the initial value. At the final stage, before breaking, the columnar kinetic energy exceeds the potential energy by 1.5 times at the peak of the spectrum. The connection between columnar energy $e_c$ and wave height $H_f$ is shown in Fig. 10. As seen, this dependence is close to an exponential one.

Details of the extreme wave development from $t=5.06$ to $t=7.15$ are given in Fig. 11. As seen, the freak wave is developing just over two wave periods. The energy in the peak column amplifies over this period of time by approximately ten times. The fast growth of the maximum value of surface velocity, normalized by phase velocity $v_m$ of the extreme wave, is shown in Fig. 11(c). It can be seen that fluid velocity approaches phase velocity before wave breaking. The evolution of energy $E_f$ averaged throughout the trough to trough interval (which is assumed to be the overall energy of the chosen wave) as well as the maximum of energy at the wave peak are given in Fig. 11(d). The most surprising feature of this picture is that the total energy of developing wave remains nearly constant (it cannot be an exact constant as a domain has open boundaries), while its peak value grows dramatically. In some other cases the total energy of certain waves is even decreasing. It proves that a freak wave goes through a self-amplification phase with no substantial exchange of energy with other waves. Therefore, any considerations of freak wave generation in Fourier space are pointless: just one wave in a wide set of similar waves unpredictably starts fastly developing accompanied by powerful concentration of energy in the vicinity of a wave peak. Evidently it is the main property of an extreme wave which makes the largest of those waves a freak one. The mechanisms of this evolution are still unknown, and the prediction of time and location of the wave development (freaking) is impossible even in a numerical experiment. Fortunately enough, such knowledge would not make any sense for practical use. Much more important is the statistics of such events and mechanical characteristics of freak waves. The above problem is similar to that of the numerical forecast of thunderstorms: the atmospherics model can predict a possibility of storm generation in a cell of the numerical model but not the exact location and time of such events.

Another type of wave evolution which was not terminated by breaking is shown in Fig. 12. In this case the columnar energy $e_c$ also concentrates around the crest and reaches very high values, but upon passing maximum values it starts to decrease, quickly returning to a normal level. It is impossible to explain why one wave comes to breaking

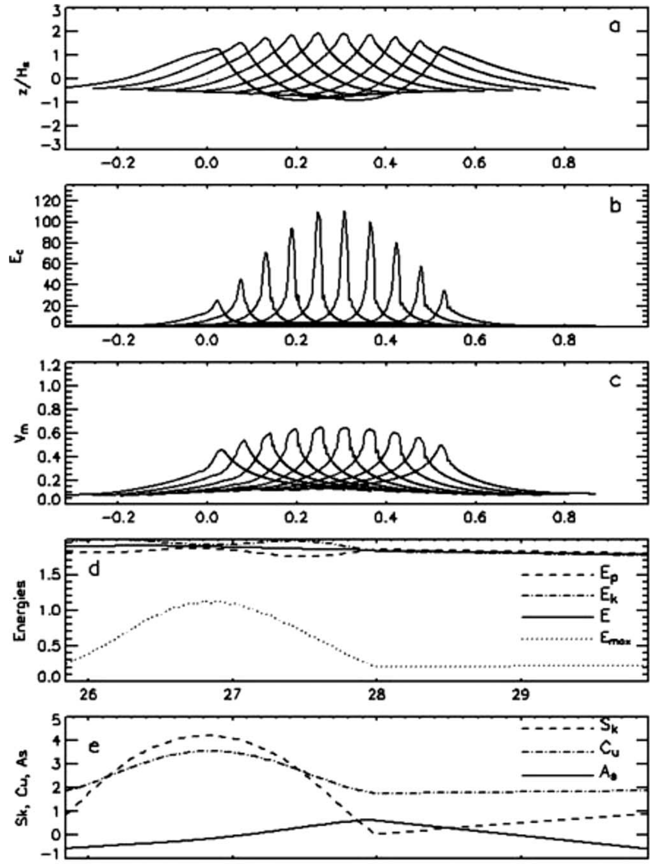


FIG. 12. The same as in Fig. 11 but for nonbreaking wave: (a) shows successive profiles (separated by interval $\Delta t$=0.08) of the largest wave within the time range from $t$=25.84 ($H_f/H_s$=2.10 at $t$=11.63 periods) up to the moment of wave height fall to the value 2.1$H_s$ at $t$=29.88 (3.22 periods). The maximum value $H_f/H_s$=2.51 was observed at $t$=27.04. All other panels for this case are the same as in Fig. 11.

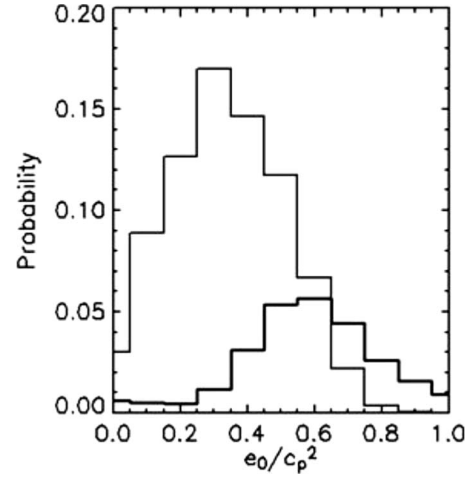


FIG. 13. Probability distribution of the surface kinetic energy (normalized by squared phase velocity $c_p^2$) of extreme waves with trough-to-crest height $H_f > 2.1$: thin line represents nonbreaking waves (1092 cases); thick line shows breaking waves (379 cases).

while another one, being even higher, can survive. Obviously, each individual development depends on details of the current environment in a physical space: in some cases group effects can initiate breaking that can start due to a very small disturbance. The final stage of this development, i.e., breaking, is characterized by a higher concentration of energy compared to the energy accumulated in the case of a surviving wave. It is clearly seen in Fig. 13 where distribution of surface energy probability for extreme waves with a trough-to-crest height $H_f > 2.1$ is shown. The probability is normalized by the total number of breaking and not breaking waves. The probability of nonbreaking waves is higher than that of breaking waves, but the maximum of surface energy is considerably shifted to higher values of extreme waves. This conclusion is also proved correct by the data presented in Fig. 14, where maximum columnar energy $E_{cm}$ and surface velocity $V_m$ (normalized by peak phase velocity $c_p$) for each case of extreme wave development are shown as a function of $H_{fn}$. The dots in this figure correspond to nonbreaking waves and asterisks to breaking waves. It is seen than most of the asterisks (but not all of them) fall mostly on the upper part of the figure. It means that large breaking waves generate higher surface velocity and dynamic pressure on the surface of floating or fixed objects; hence they are more dangerous than nonbreaking waves. Distribution of velocity on top of a breaking wave is represented in Fig. 15. It is seen that the velocity reaches the value of the phase velocity (which is an actual cause of overturning). Being observed from the upfront trough, the top of the wave looks exactly like a wall of water, The topmost part of the wave has a height $0.2H_f$ and it is really vertical. The dimensional parameters of such a wave look impressive. Let us assume that the waves and wind have reached equilibrium state and the wave spectrum is described by the PM formula. In this case, phase velocity

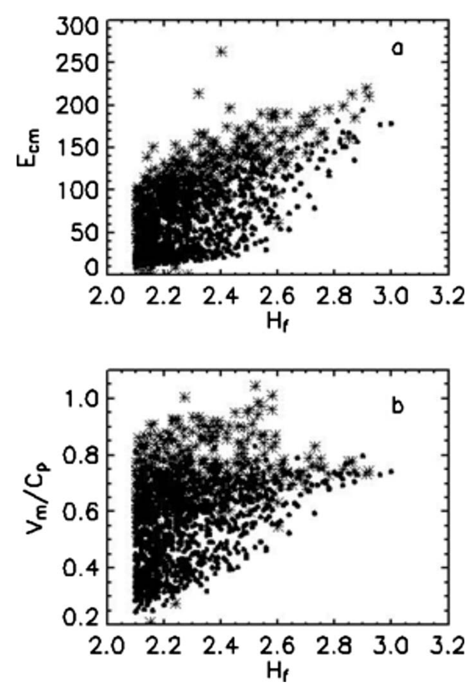


FIG. 14. All of the events when the value of trough-to-crest height is higher than 2.1$H_s$: (a) is the maximum value of columnar energy $E$ [Eq. (27)]; (b) is the maximum value of surface velocity (normalized by phase velocity $c_p$). In both panels the horizontal axis is the maximum value of extreme trough-to-crest height $H_f$. Dots correspond to nonbreaking extreme waves; asterisks show breaking extreme waves.

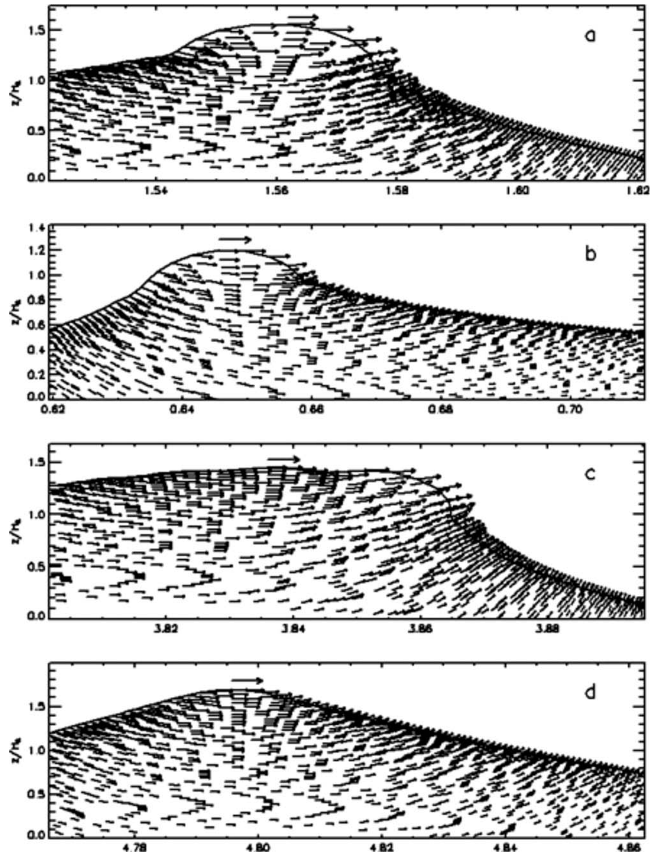


FIG. 15. Examples of extreme wave shapes and velocity fields in the top part of waves: (a) is a sharp-crested breaking wave with high asymmetry As and skewness Sk ($H_s$=0.045, $H_f$=2.36, Sk=0.84, As=4.07); (b) is a sharp-crested breaking wave with small asymmetry As and skewness Sk: ($H_s$=0.038, $H_f$=2.10, Sk=0.08, As=0.55); (c) is a flat-crested breaking wave with high asymmetry As and skewness Sk ($H_f$=0.039, $H_f$=2.16, Sk=1.06, As=4.28); (d) is a sharp-crested nonbreaking wave with medium asymmetry As and high skewness Sk ($H_s$=0.031, $H_f$=2.62, Sk=0.88, As=0.49). The arrow on top indicates phase velocity.

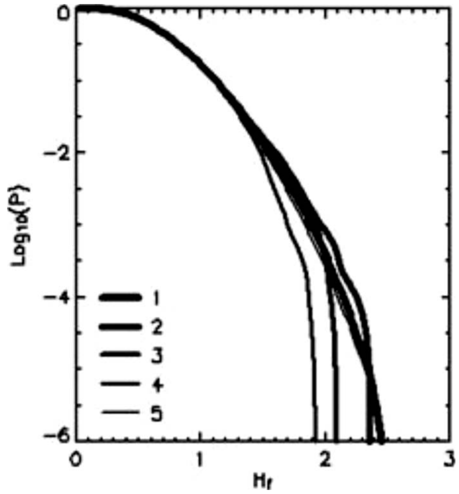


FIG. 16. Probability distribution of trough-to-crest heights calculated throughout long runs up to 2000 peak periods for the initially assigned JONSWAP/PM spectrum: 1−Ω=3 (very young sea); 2−Ω=2 (young sea); 3−Ω=0.855 (developed sea); 4−Ω=0.855, $S=0.5S_\infty$ (PM spectrum multiplied by 0.5); 5−Ω=0.855, $S=0.1S_\infty$.

$c_p$ of peak waves equals to $1.17U_{10}$, and significant wave height $H_s$ equals to $0.22U_{10}^2/g$. It follows that for $U=20$ m/s the trough to-crest extreme wave height $H_f$ equals to 23 m, for $U=25$ m/s to 35 m, and for $U=30$ m/s to 50 m. Dynamic pressure $P=\rho_w U^2$($\rho_w$ is the water density) created by moving water can reach $5.5\times10^5$, $8.6\times10^5$, and $1.2\times10^6$ Pa correspondingly. If a wave does not break, the estimations for velocity should be reduced by 1.5–2 times and for pressure by 2–4 times.

## VI. STATISTICS OF EXTREME WAVES

Figure 3 shows a slight tendency of increasing the height of extreme waves with decreasing of steepness (wave age). Probably, very energetic wave field destroys the growing waves before they reach large heights. However, it is reasonable to expect that with further decreasing of steepness the generation of extreme waves should be less intense. To check this statement, very long runs for different wave ages of the JONSWAP/PM spectrum were performed. Because of the existence of slow flux of energy to high wave number range of spectrum, the wave field gradually loses the energy. To make a long run uniform, an imitation of energy flux from the wind was added by multiplying all Fourier components $\eta_k$ and $\phi_k$ $(k=-M,M)$ at each time step by coefficient $\delta=(E_c^0/E_c)^{1/2}$, where $E_c$ is the total energy [see Eq. (26)] and $E_c^0$ is the total energy in initial conditions. A typical value of coefficient $\delta$ was 1.000 001. Because this operation changes only the integral energy, it evidently does not influence the structure of the spectrum and shapes of individual waves. The calculations were done for five cases from a very young sea ($\Omega=U/c_p=3$) up to an artificially "old" sea, the wave spectrum of which was assigned by the PM spectrum multiplied by a coefficient of 0.1. The integral probability distributions for trough-to-crest heights calculated with a moving window with length of $1.5L_p$ are given in Fig. 16 (each curve was interpolated from $H_f=0$ to $H_f=1$ with the Rayleigh formula). The results of these calculations were unexpected: the largest extreme wave with a maximum value of $H_f=2.65$ was simulated for the youngest wave field with $\Omega=3$, but a much larger number of waves with $H_f>2.5$ was found for the case $\Omega=2$. The cases $\Omega=0.855$ (PM spectrum for developed sea) and reduced by a factor of 0.5 PM spectrum gave the reasonably smaller number of extreme waves, but very gentle wave field with a spectrum of $0.1S_\infty$ (thin curve nearly coinciding with thick curve) showed the same statistics of extreme waves as the steepest wave field (thickest curve). These results convince us that the frequency of freak waves is not connected directly to the energy of the wave field, and for obtaining the representative statistics it is necessary to perform the long series of calculations for a broad range of initial conditions, characterized by the wave spectrum and by the set of initial phases. This approach was described in Sec. III. It is remarkable that the statistical properties calculated for each run were dependent not only on the shape of the initial spectrum (what is understandable) but also on the phases of the modes. For the same spectrum and different phases the statistics of rare cases can be very different: one run reproduces several extreme waves, and another does not reproduce them at all. Extreme waves can appear either in

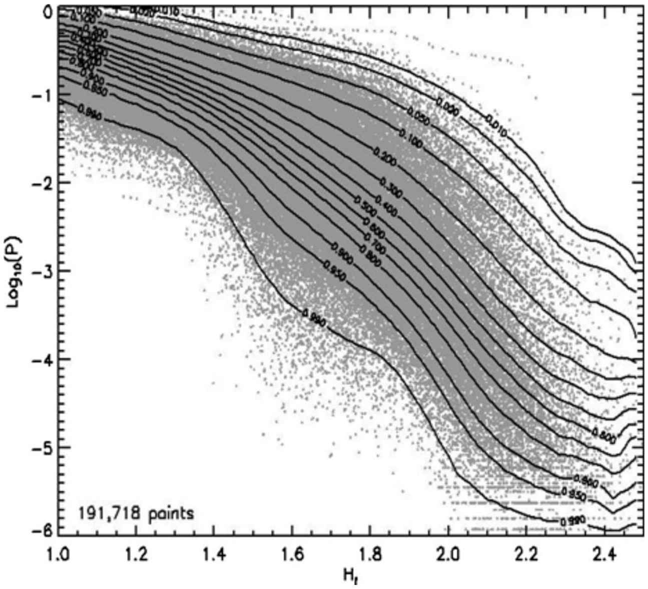


FIG. 17. Contours $P_p(P,H_f)$ corresponding to the number of cases falling into cells of sizes $\Delta H_f=0.02$ and $\Delta \log_{10}P=0.1$. Dotted line is an averaged value for each bin.

the beginning of a run or after a long time of integration. It means that the generation of an extreme wave is an essentially random process, which is initiated by very delicate and unpredictable properties of a local wave field in a physical space.

The data on integral probability $P$ of waves (probability of waves, whose crest-to-trough height exceeds $H_f$) in the interval $1<H_f<2.5$ calculated over all 4294 runs are represented in Fig. 17, where contours $P_p(P,H_f)$ correspond to the number of cases falling in cells with the sizes $\Delta H_f=0.02$ and $\Delta \log_{10} P=0.1$ (the initial distribution of the points is seen also in Fig. 18). The total number of points used for Fig. 17 is 190 337 and the number of trough-to-crest heights exceeding $H_f=2$ is 11 955. As seen, data on integral

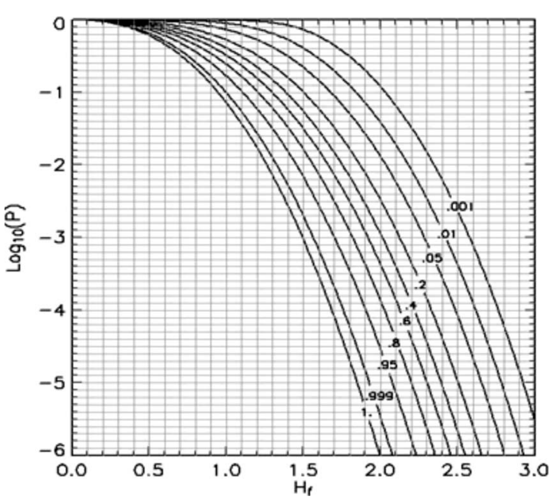


FIG. 18. Probability $P_t$ integrated over $P$ number of cases by $H_f$ bins and normalized by the total number of cases in the bins. Examples of estimations of time expectance for extreme wave values exceeding $H_f$ ($f=2.1,2.2,2.3,2.4,2.5$) for different significant wave heights $H_s$ in the range from 2 to 12 m.

probability of trough-to-crest heights have a very large scatter, which is a reflection of the random nature of the generation of extreme waves. This scatter excludes the possibility of the use of the averaged integral probability, since distribution of data inside the cloud of points should be taken into account. Attempts to stratify data in Fig. 18 over parameter $St$ [Eq. (22)] characterizing the energy of waves were unsuccessful: points corresponding to different runs obey Gauss-like random distribution inside the cloud of data (see Fig. 18). Surely, it does not mean that statistics of dimensional extreme waves does not depend on wave energy. It proves that normalizing of wave heights with significant wave height is so effective that statistics of nondimensional extreme waves tends to be independent of wave energy. In Fig. 18 is represented the probability $P_t$ integrated over $P$ number of cases $N_p$ by $H_f$ bins and normalized by total number of cases in bins,

$$P_i(P,H_f)=\frac{\Sigma_0^P N_p(P,H_f)}{\Sigma_0^{P_\infty} N_p(P,H_f)}, \tag{28}$$

where $P_\infty=10^{-6}$ was chosen. Contours of $P_i$ are plotted in Fig. 18 together with initial data on the integral probability $P$. As seen, data on $P_i$ demonstrate a regular behavior, which gives a possibility of the estimation of the distribution of probability for waves exceeding the specific value $H_f$. It is convenient instead of the probability (the frequency) of the wave to introduce the time expectance time of extreme wave $T_f$,

$$\tau_f=T_p(PP_i)^{-1}. \tag{29}$$

Examples of the estimations of the time expectance of extreme waves exceeding values $fH_s$ ($f=2.1,2.2,2.3,2.4,2.5$) for different significant wave heights $H_s$ from 2 to 12 m are given in Fig. 19. The connection between $H_s$ and $T_p$ was established with a PM spectrum, but for this purpose any wave spectrum can be used.

Vertical axes correspond to time expectance $\tau_f$ in days (logarithmic scale). A horizontal axis corresponds to the probability of meeting the wave with height $H_f$ and expectance $\tau_f$ (logarithmic scale). Different curves correspond to different $H_f$ (indicated in the legend in every frame). Thin vertical lines correspond to probability $P_t=0.5$. To make clear the use of this graphics let us give examples. If a significant wave height $H_s$ equals 4 m (top middle frame) then with probability of 0.5 the time expectance of a wave with trough-to-crest height $H_f=8.2$ m will be 0.4 day, and for $H_f=10$ m the time expectance $\tau_f=10$ days. For $H_s=10$ m and $H_f=22$ m with probability of 0.5 the expectance time $\tau_f=0.6$ days, and for $H_f=25$ m $\tau_f=20$ days. The curves in different frames in Fig. 19 look very similar due to logarithmic scales. It is a direct consequence of the universality of the probability functions for nondimensional wave heights. If the time expectance was expressed in terms of periods of peak wave $T_p$ these frames were identical. Dimensional period $T_p$ grows as $H_s^{1/2}$, and $\tau_f$ increases correspondingly.

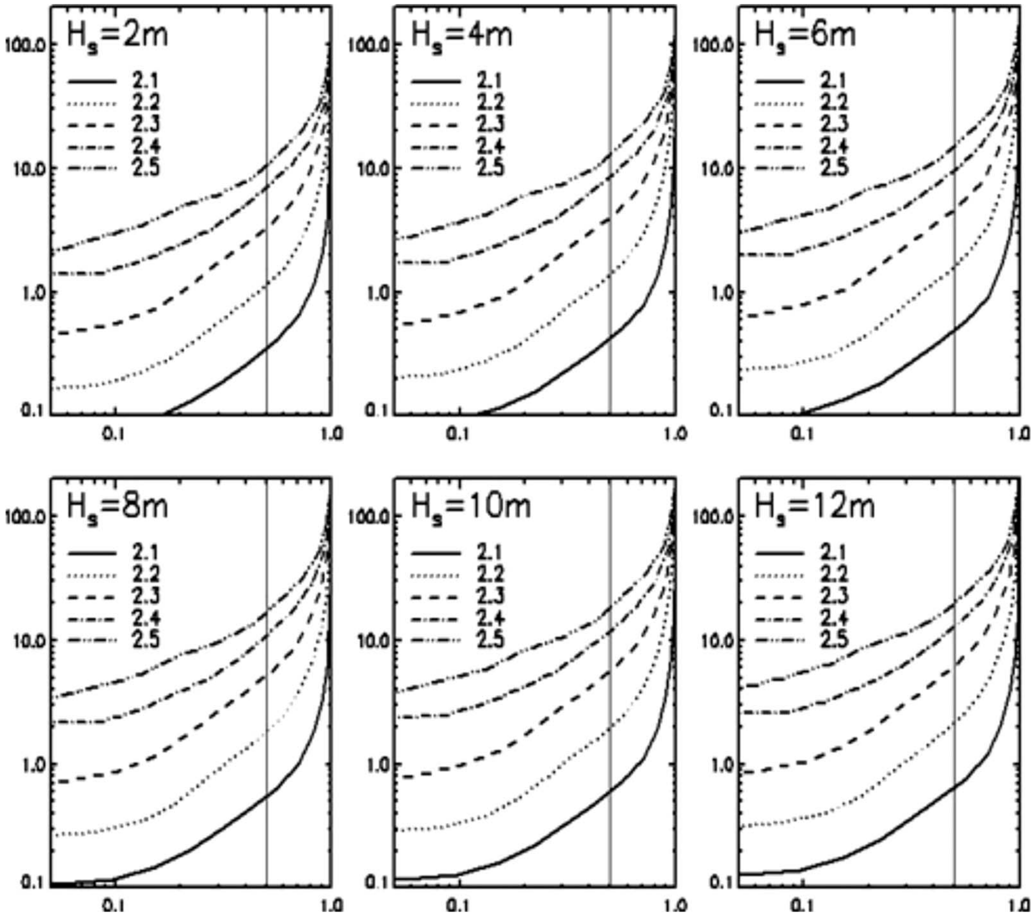


FIG. 19. Examples of estimations of time expectance for extreme wave values exceeding $H_f$ ($f=2.1,2.2,2.3,2.4,2.5$) for different significant wave heights $H_s$ in the range from 2 to 12 m.

## VII. CONCLUSIONS

Extreme wind waves are a rare though regular phenomenon in the world oceans. Such waves hold huge destruction power. Navigation, sea technologies, in particular, oil and gas production, and recreation industry persistently demand investigation of the origin and physics of extreme waves as well as the development of some techniques for their forecasting.

Mechanical properties of extreme waves and their probability and geographical distribution are still unknown, and no reliable prediction techniques still exist. Observational data on those waves are scratchy; laboratory experiments are difficult due to the extremely rare occurrence of such waves and short fetches. As the freak waves are an extraordinary phenomenon, it is unlikely that their statistics, mechanics, and a number of other quite delicate questions concerning the above problem can be investigated on the basis of various substitute equations based on expansions. Even the applicability of a potential approximation is questionable. There is also some possibility that angle spreading plays a significant role too; moreover, it seems that it decreases the probability of extreme wave generation.

A new approach to the problem is based on the methods of direct mathematical modeling that have proved to be universal in most branches of geophysical and technical fluid mechanics. For some reasons the above techniques had not been used before in statistical investigations of wave processes. Pure spectral approaches used in wave prediction models for solutions of the given problem are not suitable. Over the recent years, direct modeling of surface waves using initial fluid mechanics equations has been developed (see review in Ref. 2).

Extreme waves are as infrequent in computer simulations as in the oceans. That is why the investigation should cover a great number of numerical experiments that would be subjected to a thorough analysis. A numerical approach is based on a 2D ($x$-$z$) model of potential waves and allows obtaining rich statistical material. According to recent simulations of 3D waves made in Refs. 41 and 43 the probability of large waves increases for long-crested waves. It means that 2D simulations are a limit case of such waves. However, large waves in a stormy sea are often long crested, and a 2D approach to investigate their statistics is likely to be acceptable. This opinion is supported by the authors of the WAM (wave modeling) model,[3] in which the 1D analysis for experimental forecast of freak waves was implemented.

In this paper, the results of over 4000 numerical experiments were analyzed to investigate some properties of freak waves and calculate the probability of their appearance. Because of self-similarity of governing equations they can be used in a nondimensional form; hence, the statistical results of long-term numerical simulations depend on the following initial conditions only: profiles of elevation $\eta(x)$, surface velocity potential $\varphi(x)$, and set of initial phases. Considering practical application of the theory of rare waves, we came to the conclusion that a strict definition of freak waves in a nondimensional form is not required at all. Instead, it makes sense to introduce the categories of dimensional extreme waves, like it had been done, for example, for classifications of hurricanes. For example, the $n$th category of freak wavs can be defined as waves with trough-to-crest height equal to $3n$.

Attempts have been undertaken to stratify wave statistics over some general integral characteristics, such as skewness, kurtosis, and initial density of energy or enhancing parameter for the spectrum. The results of the above efforts turned out to be quite unexpected at first sight: in a broad range of parameters for a wind wave spectrum integral probability of freak waves was found to be virtually independent of the spectrum shape.

Finally, we arrived at the conclusion that it is naive to expect that high-order moments such as skewness and kurtosis can serve as predictors for freak waves. First, the above characteristics cannot be calculated with the use of a spectrum usually determined with low accuracy. Such calculations are definitely unstable to a slight perturbation of the spectrum. Second, even if the spectrum is determined with high accuracy (for example, calculated with the use of an exact model), the high-order moments cannot serve as the predictors, since they change synchronically with variations in extreme wave heights. The appearance of freak waves occurs simultaneously with increase in the local kurtosis; hence, kurtosis is simply a passive indicator of the same local geometrical properties of a wave field. This effect disappears completely if the spectrum is calculated over a very wide ensemble of waves (sees the Appendix). In this case the existence of a freak wave is just disguised by other waves, not freak ones. It is quite evident that kurtosis is not a predictor but an extreme wave indicator that is representative for such a small area that it can be observed as easily as a freak wave itself. A freak wave is even better recognizable than kurtosis. Third, all high-order moments are dependent on spectral presentation—they increase with increase in spectral resolution and cutoff frequency.

Statistics of nondimensional waves as well as emergence of extreme waves are the innate properties of a nonlinear wave field. The most pronounced indicator of freak waves is the freak wave itself.

The most surprising result was the discovery that the probability of nondimensional freak waves (normalized by significant wave height) is virtually independent of density of wave energy. It does not mean that the statistics of extreme waves does not depend on wave energy. It just proves that normalization of wave heights by a significant wave height is so effective that statistics of nondimensional extreme waves tends to be independent of wave energy. Wave energy is not an obvious indicator of wave field steepness. Note that defining the integral steepness is actually not so easy—any definition turns out to be dependent on the spectrum resolution, i.e., value of wave number for spectrum peak and total number of modes assigned for the description of the spectrum. This statement remains valid for routine presentation of wave field as a random superposition of linear modes. For true nonlinear waves dependence on resolution (if it is sufficiently high) should be insignificant. First, the spectrum should decrease with increase in wave number quickly enough for convergence of any important moments. Second, waves with very close wave numbers cannot run as independent waves; they would probably interact, quickly forming a single nonlinear mode. The spectrum assigned with excessively high resolution turns into a discrete spectrum.[44] A wave field is rather a superposition of a finite number of nonlinear modes distorted with random small-scale quasiturbulent noise.

The shape of freak waves varies within a wide range: some of them are sharp crested; others are asymmetric, with a strong forward inclination. The investigations show that only breaking and large waves can be referred to as freak waves. Some of them can be very big but not steep enough to create dangerous conditions for vessels (but not for fixed objects). The initial concentration of energy can occur merely as a result of group effects, but in some cases the largest wave suddenly starts to grow. The growth is followed sometimes by a strong concentration of wave energy around a peak vertical. It takes place in the course of a few peak wave periods. The process starts with an individual wave in a physical space without significant exchange of energy with the surrounding waves. Sometimes, a crest-to-trough wave height can be as large as nearly three significant wave heights. On the average, only one-third of all freak waves come to breaking, creating extreme conditions; however, if a wave height approaches the value of three significant wave heights, all of the freak waves break. Evidently, this process cannot be investigated on the basis of purely spectral equations. The phenomenon of freak waves is a manifestation of the innate properties of a nonlinear wave field, and they appear inevitably on the condition that the time of observations or numerical simulations is long enough. Individual prediction of freak waves is impossible; however, the probability of their generation can be estimated.

The current paper does not give any answer as to why freak waves occur. The problem is interesting, though it has little practical application. It can be illustrated by example from a much more developed branch of numerical geophysical fluid dynamics, i.e., large-scale atmospheric dynamics. It is well known that cyclones result from instability of baroclinic waves on frontal surfaces. It is quite difficult to predict which of many waves running on a frontal surface will start to grow and finally lose stability, becoming a freak baroclinic wave, breaking and turning into cyclone. Until now the problem of cyclogenesis remains a semiresolved problem of numerical weather forecast. Nevertheless, well developed high resolution atmospheric models predict climate probability of cyclogenesis with high accuracy.

The results of this paper can be considered as preliminary. To obtain more representative statistics of extreme waves it is necessary to perform a significantly greater number of numerical experiments with the use of a 2D model, probably using a better resolution. The disadvantage of the current approach is the termination of a run after it has reached the infinite slope (in conformal coordinates a slope is always finite). This effect can be avoided by the introduction of breaking parametrization. This algorithm performs local smoothing of the surface, connected with loss of excessive potential and kinetic energies.[13] In this paper, breaking parametrization was not introduced intentionally to avoid distortion of the statistics of extreme waves.

At the same time the most critical cases of freak wave generation can be investigated on the basis of the new 3D model for potential waves (see, for example, Refs. 19 and 20). Recently we developed another version of the 3D model based on full nonlinear equations (see the Appendix). Being implemented on massive parallel processing computers, this model is able to simulate evolution of a 2D wave field for periods of thousands (for the number of modes of about 10 000) or hundreds (for the number of modes of about 100 000) of wave peak periods. Preliminary studies show that this model is also able to simulate the appearance of freak waves. Naturally, such a type of simulations cannot generate so big ensembles as it is possible with a 2D model, and they should be performed specifically for investigation of 3D effects. A more detailed freak wave structure can be investigated on the basis of the 2D nonpotential model in conformal coordinates, the development of which is now underway. This model will allow simulation of a closed cycle of energy and momentum transformations in the wave/turbulence/current system.

Statistical processing of the results of a great number of numerical experiments allowed preliminary estimation of the probability function shape. Possible application of such data is the formulation of a forecast method for freak waves of different categories. Such forecast can be based on existing wave prediction models: WAM and the newest WAVEWATCH model. The forecast should be probabilistic. No extreme wave prediction model can guarantee a full customers' satisfaction (as you can guess, meeting with a freak wave is meant); the model can just estimate a probability of such an impressing event more or less accurately. The strategy of the forecast is similar to that of a thunderstorm probability forecast. At present, construction of a prototype of such a forecasting model looks quite realistic. The well estimated probability function can be also used for the investigation of freak wave climate: probability of such waves of different categories for the world oceans and development of recommendations for ship design and sea technologies. A deep understanding of the extreme wave problem is impossible without special observations and continuous accumulation of data.

## ACKNOWLEDGMENTS

I would like to thank my wife Olga who assisted me in preparing the manuscript for publication. I am also very thankful to the anonymous reviewers for their many comments which I found quite useful.

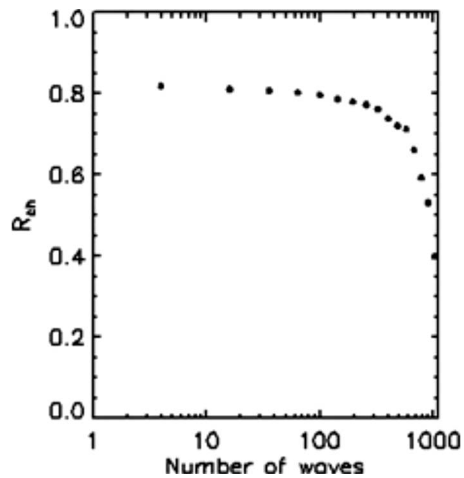


FIG. 20. Correlation coefficient between the height of the largest wave in the ensemble and the number of waves in the ensemble.

## APPENDIX: 3D MODELING

The role of ensemble size in the relationship between kurtosis and an extreme wave was investigated with the new exact model of potential waves. The model is based on the full 3D equations written in a curvilinear surface-following coordinate system: an elliptic equation for a 3D potential with full kinematic and dynamic surface boundary conditions. The numerical scheme is based on the 2D Fourier-transform method. The equation for the potential is represented as a Poisson equation with the right side including all the rest of the terms of the full elliptic equation. The equation is solved by iterations with the use of a correction of the right side. Since the equation for the surface potential and elevation includes only a vertical derivative of the potential on a surface, a stable solution was normally achieved just for several iterations. The scheme was validated by control of integral invariants and by simulation of running exact Stokes waves. The model reproduces a "horseshoe" structure and the 2D BF instability. The current version of the model takes into account 33 025 modes or $512 \times 512$ knots. The model is specifically intended for the investigation of 3D effects and nonlinear interactions between all of the modes representing a wave field. The model is suitable for effective parallelization.

The initial conditions were assigned similar to those used in Ref. 41. Amplitudes of waves with random phases were calculated with the JONSWAP spectrum for angle distribution proportional to $[\mathrm{sech}(\theta)]^4$. A peak of the spectrum was placed at wave number $\mathbf{k}=(32,10)$. By now, the calculations have been done for about 100 periods of a peak wave. The results recorded allowed to calculate the dependence of the correlation coefficient of the highest wave in domain and kurtosis calculated for the same domain for different sizes of 2D domains (expressed in squared length of the peak wave. 990 wave surfaces containing $512 \times 512$ knots were used for calculations of correlations. This dependence is shown in Fig. 20. As seen, for the smallest domain the size of which is equal to 1/256 of the entire domain, the correlation coefficient is about 0.8. The coefficient decreases down to 0.4 with increase in the domain size up to 1/4 of the entire domain. Obviously, with further increase in the domain size the connection between kurtosis and the highest wave becomes insignificant. It proves that a clear relationship between kurtosis and extreme wave for the same ensemble disappears with ensemble extension.


[1] C. Kharif and E. Pelinovsky, "Physical mechanisms of the rogue wave phenomenon," Eur. J. Mech. B/Fluids **22**, 603 (2003).
[2] K. Dysthe, H. Krogstad, and P. Muller, "Oceanic rogue waves," Annu. Rev. Fluid Mech. **40**, 287 (2008).
[3] P. Janssen, "Nonlinear four-wave interaction and freak waves," J. Phys. Oceanogr. **33**, 863 (2003).
[4] V. E. Zakharov, "Stability of periodic waves of finite amplitude on the surface of a deep fluid," J. Appl. Mech. Tech. Phys. **9**, 190 (1968).
[5] Homer, "Iliad," *The Project Gutenberg Etext of The Iliad*, translated by S. Butler (Dover, Mineola, 2000).
[6] T. B. Benjamin and J. E. Feir, "The disintegration of wave trains in deep water," J. Fluid Mech. **27**, 417 (1967).
[7] D. Chalikov, "Numerical simulation of Benjamin–Feir instability and its consequences," Phys. Fluids **19**, 016602 (2007).
[8] K. L. Henderson, D. H. Peregrine, and J. W. Dold, "Unsteady water wave modulations: Fully nonlinear solutions and comparison with the nonlinear Schrödinger equation," Wave Motion **29**, 341 (1999).
[9] K. B. Dysthe and K. Trulsen, "Note on breather type solutions of the NLS as a model for freak-waves," Phys. Scr., T **T82**, 48 (1999).
[10] A. R. Osborne, M. Onorato, and M. Serio, "The nonlinear dynamics of rogue waves and holes in deep-water gravity wave train," Phys. Lett. A **275**, 386 (2000).
[11] M. Onorato, A. R. Osborne, M. Serio, and T. Damiani, in *Rogue Waves 2000*, edited by M. Olagnon and G. A. Athanassoulis (Ifremer, Brest, France, 2000), pp. 181–191.
[12] A. Slunyaev, C. Kharif, E. Pelinovsky, and T. Talipova, "Nonlinear wave focusing on water of finite depth," Physica D **173**, 77 (2002).
[13] D. Chalikov and D. Sheinin, "Modeling of extreme waves based on equations of potential flow with a free surface," J. Comput. Phys. **210**, 247 (2005).
[14] A. Babanin, D. Chalikov, I. Young, and I. Savelyev, "Predicting the breaking onset of surface water waves," Geophys. Res. Lett. **34**, L07605, DOI:10.1029/2006GL029135 (2007).
[15] J. W. Dold and D. H. Peregrine, in *Numerical Methods for Fluid Dynamics*, edited by K. W. Morton and M. J. Baines (Oxford University Press, New York, 1986), pp. 671–679.
[16] J. W. Dold, "An efficient surface-integral algorithm applied to unsteady gravity waves," J. Comput. Phys. **103**, 90 (1992).
[17] D. Chalikov and D. Sheinin, "Numerical modeling of surface waves based on principal equations of potential wave dynamics," NOAA/NCEP/OMB Technical Note, 1996.
[18] D. Chalikov and D. Sheinin, in *Advances in Fluid Mechanics*, edited by W. Perrie (Computational Mechanics, Southampton, 1998), Vol. 17, pp. 207–258.
[19] W. J. D. Bateman, C. Swan, and P. H. Taylor, "On the efficient numerical simulation of directionally spread surface water waves," J. Comput. Phys. **174**, 277 (2001).
[20] D. Clamond and J. Grue, "A fast method for fully nonlinear water wave computations," J. Fluid Mech. **447**, 337 (2001).
[21] D. Fructus, D. Clamond, J. Grue, and O. Kristiansen, "An efficient model for three-dimensional surface wave simulations: Part I: Free surface problem," J. Comput. Phys. **205**, 665 (2005).
[22] W. T. Tsai and D. K. P. Yue, "Computation of nonlinear free-surface flows," Annu. Rev. Fluid Mech. **28**, 249 (1996).
[23] J.-B. Song and M. L. Banner, "On determining the onset and strength of breaking for deep water waves. Part I.: Unforced irrotational wave groups," J. Phys. Oceanogr. **32**, 2541 (2002).
[24] G. D. Crapper, "An exact solution for progressive capillary waves of arbitrary amplitude," J. Fluid Mech. **96**, 417 (1957).
[25] G. D. Crapper, *Introduction to Water Waves* (Wiley, Chichester, 1984).
[26] G. G. Stokes, "On the theory of oscillatory waves," Trans. Cambridge Philos. Soc. **8**, 441 (1847).
[27] J. C. Whitney, "The numerical solution of unsteady free-surface flows by conformal mapping," in *Proceedings of the Second International Conference on Numerical Fluid Dynamics*, edited by M. Holt (Springer-Verlag, Berlin, 1971), pp. 458–462.
[28] L.V. Ovsyannikov, "Dinamika sploshnoi sredy," M.A. Lavrent'ev Institute of Hydrodynamics Sib. Branch USSR Acad. Sci. **15**, 104 (1973).
[29] T. Kano and T. Nishida, "Sur le ondes de surface de l'eau avec une justification mathematique des equations des ondes en eau peu profonde," J. Math. Kyoto Univ. **19**, 335 (1979).
[30] B. Fornberg, "A numerical method for conformal mapping," SIAM J. Sci. Stat. Comput. **1**, 386 (1980).
[31] S. Tanveer, "Singularities in water waves and Rayleigh–Taylor instability," Proc. R. Soc. London, Ser. A **435**, 137 (1991).
[32] S. Tanveer, "Singularities in the classical Rayleigh–Taylor flow: Formation and subsequent motion," Proc. R. Soc. London, Ser. A **441**, 501 (1993).
[33] D. Sheinin and D. Chalikov, "Hydrodynamical modeling of potential surface waves: Problems of hydrometeorology and environment on the eve of XXI century," in *Proceedings of International Theoretical Conference*, St. Petersburg, Russia, 24–25 June 1999 (Hydrometeoizdat, St.-Petersburg, 2001), pp. 305–337.
[34] V. E. Zakharov, A. I. Dyachenko, and A. O. Prokofiev, "New method for numerical simulation of a nonstationary potential flow of incompressible fluid with a free surface," Eur. J. Mech. B/Fluids **21**, 283 (2002).
[35] V. E. Zakharov, A. I. Dyachenko, and A. O. Prokofiev, "Freak waves as nonlinear stage of Stokes wave modulation instability," Eur. J. Mech. B/Fluids **25**, 677 (2006).
[36] M. S. Longuet-Higgins and M. Tanaka, "On the crest instabilities of steep surface waves," J. Fluid Mech. **336**, 51 (1997).
[37] D. Chalikov, "Statistical properties of nonlinear one-dimensional wave fields," Nonlinear Processes Geophys. **12**, 1 (2005).
[38] M. Onorato, A. R. Osborne, M. Serio, L. Cavaleri, C. Brandini, and C. T. Stansberg, "Observations of strongly non-Gaussian statistics for random sea surface gravity waves in wave flume experiments," Phys. Rev. E **70**, 067302 (2004).
[39] M. Onorato, A. R. Osborn, and M. Serio, "Modulational instability and non-Gaussian statistics in experimental random water-wave tank," Phys. Fluids **17**, 078101 (2005).
[40] J. W. McLean, "Instabilities of finite-amplitude water waves," J. Fluid Mech. **114**, 315 (1982).
[41] M. Onorato, T. Waseda, A. Toffoli, L. Cavaleri, O. Gramstad, P. A. E. M. Janssen, T. Kinoshita, J. Monbaliu, N. Mori, A. R. Osborne, M. Serio, C. T. Stansberg, H. Tamura, and K. Trulsen, "Statistical properties of directional ocean waves: The role of the modulational instability in the formation of extreme events," Phys. Rev. Lett. **102**, 114502 (2009).
[42] A. V. Babanin and Yu. P. Soloviev, "Field investigation of transformation of the wind wave frequency spectrum with fetch and the stage of development," J. Phys. Oceanogr. **28**, 563 (1998).
[43] A. I. Dyachenko and V. E. Zakharov, "Modulation instability of Stokes wave–freak wave," Pis'ma Zh. Eksp. Teor. Fiz. **81**, 318 (2005).
[44] V. E. Zakharov and A. O. Korotkevich, A. N. Pushkarev, and A. I. Dyachenko, "Mesoscopic wave turbulence," JETP Lett. **82**, 487 (2005).